

Role Of Phosphorylation Of the Oxysterol Binding Protein (OSBP) in (PI(4)P) and Sterol-  
Containing Membrane Recognition and Binding

Hasam Madarati

A thesis submitted to the Department of Chemistry,

Centre for Biotechnology

in partial fulfillment of the requirements for the

degree of Master of Science (MSc)

Brock University

St. Catharines, Ontario

March, 2016

© Hasam Madarati, 2016

## ABSTRACT

Studies have demonstrated that the oxysterol binding protein (OSBP) acts as a phosphatidylinositol phosphate (PIP)-sterol exchanger at membrane contact sites (MCS) of the endoplasmic reticulum (ER) and Golgi. OSBP is known to pick up phosphatidylinositol-4-phosphate (PI(4)P) from the ER, transfer it to the *trans*-Golgi in exchange for a cholesterol molecule that is then transferred from the *trans*-Golgi to the ER. Upon further examination of this pathway by Ridgway et al. (1), it appeared that phosphorylation of OSBP played a role in the localization of OSBP. The dephosphorylation state of OSBP was linked to Golgi localization and the depletion of cholesterol at the ER. To mimic the phosphorylated state of OSBP, the mutant OSBP-S5E was designed by Ridgway et al. (1).

The lipid and sterol recognition by wt-OSBP and its phosphomimic mutant OSBP-S5E were investigated using immobilized lipid bilayers and dual polarization interferometry (DPI). DPI is a technique in which the protein binding affinity to immobilized lipid bilayers is measured and the binding behavior is examined through real time. Lipid bilayers containing 1,2-dioleoyl-sn-glycero-3-phosphocholine (DOPC) and varying concentrations of PI(4)Ps or sterols (cholesterol or 25-hydroxycholesterol) were immobilized on a silicon nitride chip. It was determined that wt-OSBP binds differently to PI(4)P-containing bilayers compared to OSBP-S5E. The binding behavior suggested that wt-OSBP extracts PI(4)P and the change in the binding behavior, in the case of OSBP-S5E, suggested that the phosphorylation of OSBP may prevent the recognition and/or extraction of PI(4)P.

In the presence of sterols, the overall binding behavior of OSBP, regardless of phosphorylation state, was fairly similar. The maximum specific bound mass of OSBP to

sterols did not differ as the concentration of sterols increased. However, comparing the maximum specific bound mass of OSBP to cholesterol with oxysterol (25-hydroxycholesterol), OSBP displayed nearly a 2-fold increase in bound mass. With the absence of the wt-OSBP-PI(4)P binding behavior, it can be speculated that the sterols were not extracted.

In addition, the binding behavior of OSBP was further tested using a fluorescence based binding assay. Using 22-(*N*-(7-nitrobenz-2-oxa-1,3-diazol-4-yl)amino)-23,24-bisnor-5-cholen-3 $\beta$ -ol (22-NBD cholesterol), wt-OSBP a one site binding dissociation constant  $K_d$ , of  $15 \pm 1.4$  nM was determined. OSBP-S5E did not bind to 22-NBD cholesterol and  $K_d$  value was not obtained.

## ACKNOWLEDGEMENTS

*“Your Lord has decreed: ‘The more you thank Me, the more I give you.’” Qur’an 14:7*

*My parents, Dr. Mohamad Yahya Madarati and Nawal Fattal – for their unconditional and blessed support, love and care; and of course for being patient with me on finishing this project*

*My fiancé, Sana Birawi – for her continuous motivation and “hand-in-hand” support*

*My family – for their unconditional and blessed love, support and care*

*My supervisor, Dr. Jeffrey Atkinson – for his inspiring mentorship and incredible and remarkable guidance inside and outside of the research field*

*My committee, Dr. Tony Yan and Dr. Alan Castle – for their commitment and evaluation of this work along with their incredible guidance and feedback*

*My internal examiner, Dr. Thad Harroun – for taking the role of an internal examiner and evaluating this work at such a short notice*

*My lab mate, “Dr.” Parthajit Mukherjee – for being like a brother to me on this lab and for his guidance and support on all experimental work including providing me with all of the wt-OSBP data*

*The Mukherjee family – for their continuous support and being like a second family to me*

*My lab mate, Dr. Matilda Baptist – for always providing me the extra hand in the time of need*

*My lab mate, Dr. Candace Panagabko – for mentoring me at the early stages of laboratory experiences*

*My chemistry lab mates, Mikel Ghelfi, Andrew Hildering and Nick Krueger – for educating me on everything that was chemistry related*

*Dr. Yan’s lab members, Sina Mazinani and Emily Sappendel – for their support inside the lab and the memorable times made outside the lab*

*Our collaborator, Dr. Neale Ridgway – for providing us with baculovirus samples and being patient with us during troubleshooting*

*Brock University and NSERC – for making this opportunity happen*

*Everyone else who has taken the time to read, edit, comment, and listen to my research work*

## TABLE OF CONTENTS

<b>1. INTRODUCTION</b>	<b>PAGE</b>
1.1. Lipids.....	1
1.2. Membrane Contact Sites (MCS).....	5
1.3. OSBP-Related Proteins (ORP).....	7
1.3.1. Yeast OSBP Homologue (Osh4p/Kes1p).....	7
1.3.2. Oxysterol Binding Protein (OSBP).....	11
1.4. Protein Phosphorylation.....	16
1.5. Overview of Project.....	19
<b>2. MATERIALS AND METHODS</b>	
2.1. Consumable Products.....	21
2.2. Chemical Reagents and Solutions.....	21
2.2.1. Enzymes and Antibiotics.....	21
2.2.2. Baculoviruses and Insect Cells.....	22
2.2.3. Culture Medium and Buffers.....	22
2.2.3.1. Culture Medium.....	22
2.2.3.2. OSBP Purification Buffers.....	23
2.2.3.3. Sodium Dodecyl Sulphate (SDS) Polyacrylamide Gel Electrophoresis.....	23
2.2.3.4. Ion Exchange Chromatography Buffer.....	24
2.2.3.5. Dual Polarization Interferometry (DPI) Buffer.....	24
2.2.3.6. Fluorescence Based Assay Buffers.....	24
2.3. Equipment and Software.....	24
2.4. Experimental Protocols.....	26
2.4.1. Growth of Sf21 Cells.....	26
2.4.2. Preparation of Sf21 Freeze Stock Cultures.....	27
2.4.3. Baculovirus Infection of Sf21 Cells (Expression of OSBP and Baculovirus).....	28
2.4.4. Preparation of Resin for Column Chromatography.....	28
2.4.5. Purification of OSBP.....	29
2.4.6. Protein Quantification.....	31
2.4.7. SDS-PAGE Electrophoresis.....	31

2.4.8. Buffer Exchange.....	33
2.4.9. Ion-Exchange Chromatography.....	34
2.4.10. Preparation of Unilamellar Vesicle .....	34
2.4.10.1. Preparation of Large Unilamellar Vesicle (DPI Lipids).....	34
2.4.11. Dual Polarization Interferometry – Membrane Lipid-Protein Binding Assay.....	35
2.4.12. Fluorescence Based Assays.....	37
2.4.12.1. Ligand Binding Assay.....	37

### **3. RESULTS AND DISCUSSION**

3.1. Growth of Sf21 Cells.....	38
3.2. Baculovirus Infection of Sf21 Cells (Expression of OSBP and Baculovirus).....	43
3.3. Purification of OSBP.....	45
3.4. OSBP Quantification.....	48
3.5. Ion-Exchange Chromatography.....	50
3.6. DPI – Membrane Lipid-Protein Binding Assay.....	54
3.7. Fluorescent Based Assays.....	63
3.7.1. Binding Assay.....	63

### **4. CONCLUSION AND FUTURE DIRECTIONS.....**

### **5. REFERENCES.....**

## LIST OF TABLES

No.		PAGE
Table 1:	SDS-PAGE gel recipe.....	32
Table 2:	Recovery of OSBP-S5E: Protein concentration and amount.....	50

## LIST OF FIGURES

No.		PAGE
Figure 1:	Chemical structures and IUPAC names of different lipids.....	2
Figure 2:	Chemical structure of phosphatidylcholine (PC).....	3
Figure 3:	Basic phospholipid chemical structure.....	3
Figure 4:	Chemical structure of 1,2-dioleoyl- <i>sn</i> -glycero-3-phosphocholine (DOPC)...	4
Figure 5:	Chemical structure of cholesterol and the oxysterol 25-OH cholesterol.....	5
Figure 6:	Sequence alignment of Osh proteins.....	8
Figure 7:	Ribbon protein structure of Osh4p/Kes1p.....	9
Figure 8:	Proposed PI(4)P-sterol exchange pathway for the Osh4p.....	10
Figure 9:	Sequence alignment of human OSBP/ORP proteins.....	12
Figure 10:	Proposed PI(4)P-sterol exchange pathway for the OSBP.....	13
Figure 11:	Organization of OSBP domains between the ER and Golgi.....	14
Figure 12:	Mutations at different phosphorylation sites of OSBP.....	18
Figure 13:	Chemical structure of phosphorylated serine and glutamic acid.....	18
Figure 14:	Sf21 monolayer culture after sub-culturing (Day 0).....	39
Figure 15:	Sf21 monolayer culture after 2 days of growth.....	39
Figure 16:	Sf21 monolayer culture prior to being sub-cultured (Day 4).....	40
Figure 17:	Sf21 suspension culture prior to being sub-cultured (Day 4).....	40
Figure 18:	Sf21 suspension culture infected with OSBP-S5E baculovirus (Day 3).....	44
Figure 19:	Sf21 suspension culture infected with OSBP-S5E baculovirus obtained from filtered supernatant of a pre-infected culture (Day 3).....	44
Figure 20:	FPLC characteristics of low expression of S5E.....	46
Figure 21:	FPLC characteristics of good expression of S5E.....	47
Figure 22:	SDS-PAGE of OSBP-S5E purification by cobalt affinity column.....	48
Figure 23:	Bradford assay calibration curve.....	49
Figure 24:	SDS-PAGE of OSBP-S5E purification by ion exchange chromatography...	53
Figure 25:	Real time association curves of wt-OSBP and OSBP-S5E with DOPC bilayer.....	55
Figure 26:	Maximum adsorbed mass of wt-OSBP and OSBP-S5E to DOPC bilayer...	56

Figure 27:	Real time association curves of wt-OSBP with varying concentrations of PI(4)P bilayers.....	57
Figure 28:	Real time association curves of OSBP-S5E with varying concentrations of PI(4)P bilayers.....	58
Figure 29:	Real time association curves of wt-OSBP with varying concentrations of cholesterol bilayers.....	59
Figure 30:	Real time association curves of OSBP-S5E with varying concentrations of cholesterol bilayers.....	60
Figure 31:	Real time association curves of wt-OSBP with varying concentrations of oxysterol bilayers.....	61
Figure 32:	Real time association curves of OSBP-S5E with varying concentrations of oxysterol bilayers.....	61
Figure 33:	Maximum bound mass of OSBP with increasing molecular percentage of ligand.....	62
Figure 34:	Binding assay of wt-OSBP and OSBP-S5E with 22-NBD-cholesterol.....	64
Figure 35:	Normalized data of binding assay of wt-OSBP with 22-NBD-cholesterol...	65

## ABBREVIATIONS

$\alpha$ -TTP	$\alpha$ -tocopherol transfer protein
ADP	Adenosine diphosphate
APS	Ammonium persulfate
ARF1-GTP	ADP-ribosylation factor 1 – guanine nucleotide-binding protein
ATP	Adenosine triphosphate
BSA	Bovine serum albumin
CERT	Ceramide transfer protein (ceramide transporter)
DEAE	Diethylaminoethane
DMSO	Dimethyl sulfoxide
DOPC	1,2-dioleoyl-sn-glycero-3-phosphocholine
DOPS	1, 2-dioleoyl-sn-glycero-3-phospho-L-serine
DPI	Dual polarization interferometry
DTT	Dithiothreitol
EDTA	Ethylenediaminetetraacetic acid
EtOH	Ethanol
ER	Endoplasmic reticulum
FAPP2	Four-phosphate adaptor protein 2 (glucosylceramide transporter)
FBS	Fetal bovine serum
FFAT	Two phenylalanines in acidic tract
FRET	Fluorescence (Förster) resonance energy transfer
FPLC	Fast protein liquid chromatography
G6P	Glucose-6-phosphate
GOLD	Golgi dynamics domain
HCl	Hydrochloric acid
IEC	Ion exchange chromatography
IMAC	Immobilized-metal affinity chromatography
IPA	Isopropanol
K <sub>d</sub>	Dissociation constant
LB	Luria-Bertani
LTP	Lipid transport protein

LUV	Large unilamellar vesicle
MCS	Membrane contact sites
MES	2-(N-morpholino)ethanesulphonic acid
MOI	Multiplicity of infection
NaCl	Sodium chloride
NBD-Cholesterol	22-(N-(7-nitrobenz-2-oxa-1,3-diazol-4-yl)amino)-23,24-Bisnor-5-cholen-3 $\beta$ -ol
ORD	OSBP-related domain (also referred to as SBD – sterol binding domain)
ORP	OSBP-related protein
OSBP	Oxysterol binding protein
OSBP-wt	Oxysterol binding protein – wild type
OSBP-S5E	Oxysterol binding protein mutant S5E (5 serine residues mutated to glutamic acids)
PBS	Phosphate buffered saline
PC	Phosphatidylcholine
PE	Phosphatidylethanolamine
PH	Pleckstrin homology domain
PI	Phosphatidylinositol
PIP	Phosphatidylinositol phosphate
PI(4)P	Phosphatidylinositol-4-phosphate
PI(4,5)P <sub>2</sub>	Phosphatidylinositol-4,5-diphosphate
PM	Plasma membrane
PMCA	Plasma membrane Ca <sup>2+</sup> ATPase
PS	Phosphatidylserine
RB	Running buffer
RyR	Ryanodine receptors
SB	Salt buffer
SBD	Sterol binding domain (also referred to as ORD – OSBP-related domain)
SDS	Sodium dodecyl sulfate

SDS-PAGE	Sodium dodecyl sulfate polyacrylamide gel electrophoresis
SERCA	Sarcoplasmic/endoplasmic reticulum Ca <sup>2+</sup> ATPase
Sf21	<i>Spodoptera frugiperda</i> line 21
SFM	Serum-free media
SM	Sphingomyelin
TEMED	Tetramethylethylenediamine
VAMP	Vesicle associated membrane protein
VAP-A	VAMP associated protein A

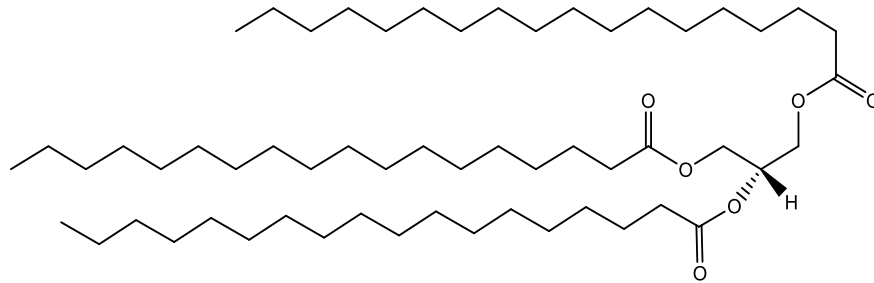
# 1. INTRODUCTION

## 1.1. Lipids

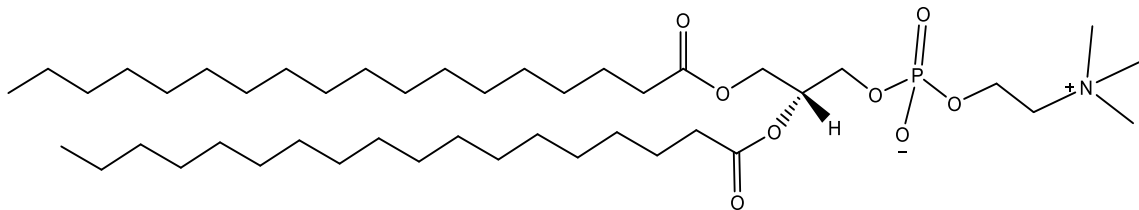
Lipids are a group of naturally occurring molecules that include fats, sterols, glycerides, phospholipids and more (Figure 1) (2). With various biological functions, lipids have important roles in energy storage, as structural components of membranes, in cell signaling, and more (3). Although the majority of lipids are categorized as hydrophobic molecules, there are some lipids, such as phospholipids, that are categorized as amphiphilic. The amphiphilic nature of phospholipids allows them to form unilamellar/multilamellar vesicular membranes. Small unilamellar vesicles (SUVs) can range up to 100 nm in size (3). Phospholipids, more precisely glycerophospholipids, similar to glycerides, possess a glycerol backbone esterified to fatty acid chains. However, unlike triglycerides, phospholipids possess a phosphate group and a head group, e.g. choline in the case of phosphatidylcholine (PC), instead of the third fatty acid chain, giving them their amphiphilic property (Figure 2) (4). Cellular membranes consist mostly of double layered phospholipids arranged in such a way that the acyl chains of the fatty acids are facing each other on the inside and the head groups are facing the outside on both surfaces (3).

The first phospholipid, identified by Gobley from the egg yolk of chickens, was lecithin or phosphatidylcholine (PC) (5). Due to the structure of choline, PC becomes zwitterionic, hence characterizing PC as a neutral phospholipid (Figure 3) (6). Other common phospholipids exist in a net anionic form due to the lack of charge in the substituent to the head group, such as in the case of phosphatidylinositol (PI) (Figure 3) or the charged but net neutral head group of phosphatidylserine (PS) (6). Studies involving phospholipids

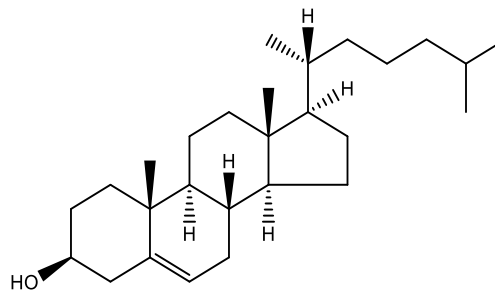
have commonly incorporated the use of unsaturated fatty acid chain lipids, such as 1,2-dioleoyl-*sn*-glycero-3-phosphocholine (DOPC) instead of the most prevalent PC lipid (Figure 4) (7).



The Triglyceride - Stearin - 2,3-di(octadecanoyloxy)propyl octadecanoate



The Phospholipid - PC - 1-stearoyl-2-stearoyl-phosphatidylcholine



The Sterol - Cholesterol - (3 $\beta$ )-cholest-5-en-3-ol

Figure 1: The chemical structures and IUPAC names of the triglyceride stearin, the phospholipid PC and the sterol cholesterol (2).

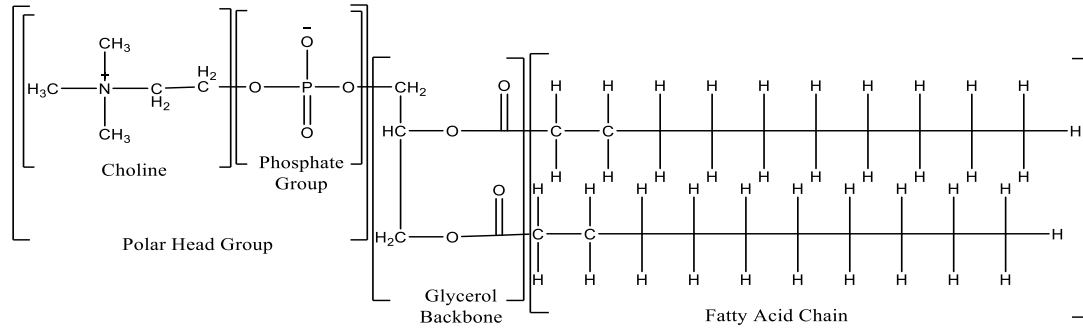


Figure 2: The chemical structure of the phospholipid phosphatidylcholine (PC) and its major groups (adapted from Featherstone, (4)).

Basic phospholipid structure	Substituent (X)	Phospholipid/Characteristic
		<b>hydrogen</b> <b>PA</b> <b>anionic</b>
		<b>ethanolamine</b> <b>PE</b> <b>zwitterionic</b>
		<b>choline</b> <b>PC</b> <b>zwitterionic</b>
		<b>serine</b> <b>PS</b> <b>anionic</b>
		<b>glycerol</b> <b>PG</b> <b>anionic</b>
		<b>phosphatidylglycerol</b> <b>CL</b> <b>anionic</b>
		<b>inositol</b> <b>PI</b> <b>anionic</b>

Figure 3: The basic phospholipid chemical structure and its characteristic based on different substituents (6).

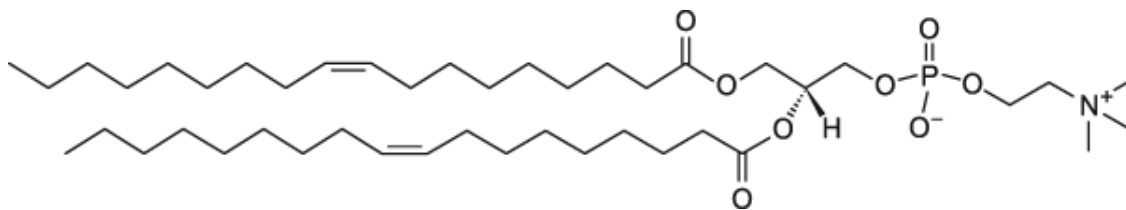


Figure 4: The chemical structure of 1,2-dioleoyl-*sn*-glycero-3-phosphocholine (DOPC) (7).

Cellular membranes vary in phospholipid content and composition from one cell to another. In fact, membranes within the cell also vary. Although the phospholipid composition of the membranes is known, the influence this composition has on cellular properties is not completely understood. The current hypotheses proposed are that certain cells and proteins require specific membranes in order to maintain functional properties (8). Mammals contain a high proportion (40-80% of dried cell weight) of phospholipids (8). The major phospholipids in mammalian membranes are phosphatidylcholine (PC), followed by phosphatidylethanolamine (PE) (8). Other lipids such as cholesterol and sphingomyelin are also found in plasma membranes (8). For example, the amount of cholesterol present in the endoplasmic reticulum (ER) membrane is 3-6% of total lipids (9).

Whilst the ER membrane is poor in cholesterol, the ER is also the location where cholesterol is synthesized (10). This is indicative that this sterol is being transferred by some means to nearby compartments. Studies have shown that the oxysterol binding protein (OSBP) transfers cholesterol, and the oxidized sterol 25-hydroxy cholesterol (oxysterol) (Figure 5), between the ER and the Golgi (10). This process is coupled with phosphatidylinositol-4-phosphate (PI(4)P) exchange at membrane contact sites (MCSs) (10).

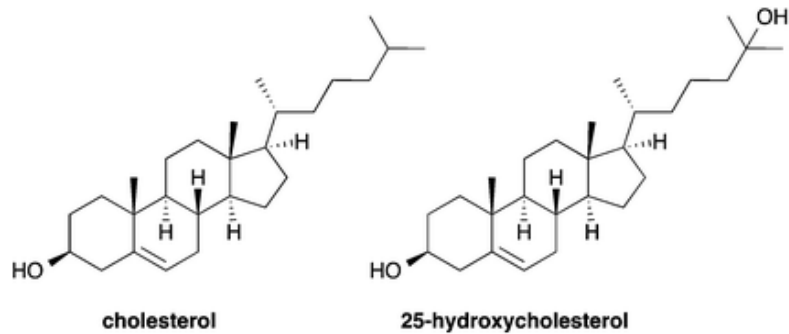


Figure 5: The chemical structure of cholesterol in comparison to its oxidized form 25-OH cholesterol (2).

## 1.2. Membrane Contact Sites (MCS)

Membrane contact sites (MCS) are narrow cytoplasmic gaps in which organelles come to close proximity, around 30 nm or less (11; 12). With close proximity, organelles can exchange relatively small molecules such as ions and simple lipids between two compartments. MCS can be involved in various processes including regulation of immune response, apoptosis, organelle dynamics and much more (11). On a molecular level, MCS are involved with calcium ( $\text{Ca}^{2+}$ ) and/or lipid exchange between compartments mainly around the ER (11). The ER is the main site of lipid synthesis and the main storage of cellular  $\text{Ca}^{2+}$  (11).

Starting with calcium signaling, the concentration of  $\text{Ca}^{2+}$  in the ER is  $10^6$  times greater to that of the concentration of  $\text{Ca}^{2+}$  in the cytosol (the ER concentration is in the millimolar range while the cytosol concentration is in the nanomolar range) (13). The difference in the concentration of calcium and the presence of SERCA (Sarcoplasmic/Endoplasmic Reticulum  $\text{Ca}^{2+}$  ATPases which pump  $\text{Ca}^{2+}$  into the ER) and

PMCA (Plasma Membrane  $\text{Ca}^{2+}$  ATPases which pump  $\text{Ca}^{2+}$  out of the cell) creates a gradient that is used in signaling events by activating downstream  $\text{Ca}^{2+}$ -binding proteins using  $\text{Ca}^{2+}$  channels (example the Ryanodine Receptors (RyR)) (11; 13). Examples of such events include processes of memory, vision, muscle contraction, immune response and much more (13). In addition and on a smaller scale, cytosolic microdomains are formed with slow  $\text{Ca}^{2+}$  diffusion, where the concentration of  $\text{Ca}^{2+}$  differs to that of the bulk cytosol (11). Microdomains are created at MCS in which coordinate the majority of the  $\text{Ca}^{2+}$  movements across different compartments (11).

Lipid exchange is prominent at the ER where most lipids are synthesized. Some lipids, such as cholesterol and ceramide can be transported even in the absence of a vesicular transport system (12). MCS is thought to play a role in facilitating lipid exchange between paired organelles by ensuring the specificity and efficacy of the lipid exchange (11; 14). In a non-vesicular transport system, lipids are transported via lipid transport proteins (LTP), such as in the example of OSBP which interacts with MCS of the ER (11). The LTP OSBP is able to extract one lipid molecule from one membrane and transfer it to another; in this case PI(4)P is extracted from the ER and transferred to the Golgi (11). LTPs are known to have domains that tend to interact with different membranes; in the case of OSBP, OSBP has a PH (Pleckstrin Homology) domain that interacts with PI(4)P at the Golgi and a FFAT motif that interacts with VAP-A at the ER (more detail on the domains of OSBP and OSBP pathway is explained in the upcoming sections) (11; 15). LTPs' targeting domains are directed to MCS of different membranes and it is believed that MCS provides specificity to the LTP's binding to lipid membranes.

### **1.3. OSBP-Related Proteins (ORP)**

ORPs are a family of cytosolic lipid transfer proteins that were found after the discovery of the OSBP (16). In addition to their lipid binding and transfer ability, ORP proteins have an affinity for cholesterol and oxysterols (17). ORP proteins are identified by their OSBP fingerprint sequence EQVSHHPP, identified in yellow in the figures below (Figure 6 and 9) (18; 19). The most common feature of ORP proteins is the sterol binding domain (SBD), also known as the OSBP related domain (ORD) (17). ORD is a  $\beta$ -barrel sterol-binding domain that is conserved from yeast to humans (17; 20). Other domains that may be found in ORPs are the Pleckstrin Homology (PH) domain that is responsible for sensing and binding to the phospholipid PI(4)P, FFAT (two phenylalanines in an acidic tract) that is responsible for sensing and binding to vesicle associated proteins (VAP) located at the ER, GOLD (Golgi domains) and ankyrin repeats (21). Since the discovery of OSBP, a total of 12 proteins have been associated with ORP family of proteins (20). The yeast homologues of OSBP, the Osh family of proteins, have been extensively studied in order to better understand the behavior of the sterol binding proteins.

#### **1.3.1. Yeast OSBP Homologue Osh4p/Kes1p**

The yeast *S. cerevisiae* has seven OSBP homologues (Osh1p-Osh7p) (17). In addition to all Osh proteins having an OSBP fingerprint sequence and the ORD, a few (Osh1p-Osh3p) have a Pleckstrin Homology (PH) domain (Figure 6) (19). The simplest and most studied homologue is Osh4p/Kes1p. Due to the inability of crystallizing the human OSBP, Osh4p was isolated and crystallized by Im *et al.* at 1.5-1.9 Å resolution (Figure 7) (21). The structure of Osh4p is built around a  $\beta$ -barrel center that consists of 19 antiparallel

$\beta$ -sheet strands (residues 115-293) (Figure 7) (21). The structure of the  $\beta$ -barrel is oriented in a way that allows the protein to have a hydrophilic exterior and a hydrophobic tunnel on the interior (21). The N-terminal (residues 1-29) act as a lid that remains unfolded leaving the barrel pocket open when the protein is without a ligand (21). Upon sterol binding, the lid closes and the sterol becomes bound in a head-down orientation in which the hydroxyl group of the sterol is buried at the bottom of the barrel (21). This, in accordance with non-vesicular transport, is how sterols move from plasma membrane (PM) to ER (22). Investigations have shown that Osh4p is capable of sterol transport among cellular compartments and is, in fact, regulated by phosphoinositides, specifically phosphatidylinositol-phosphates (PIPs) (22; 23).

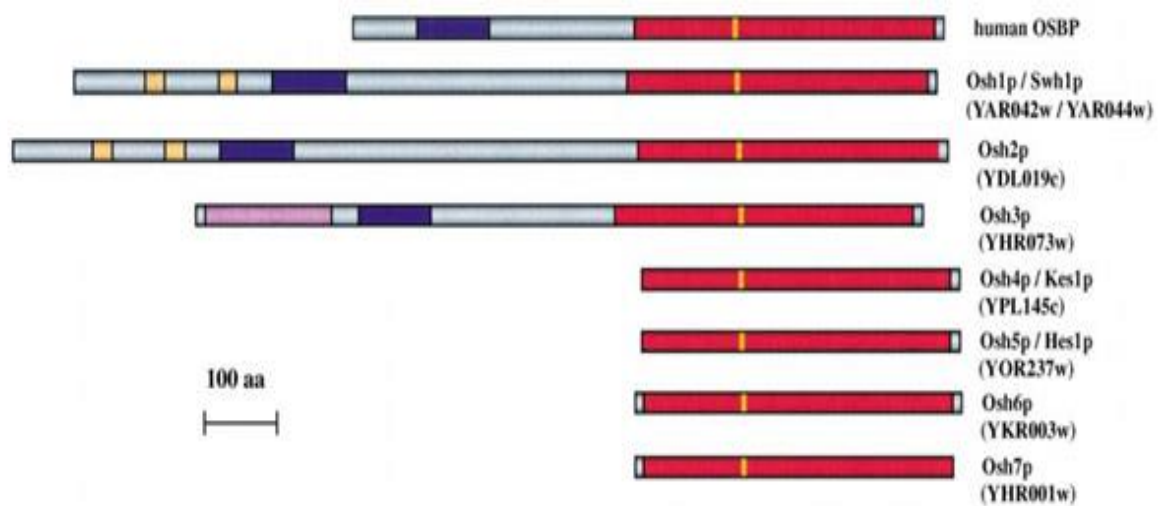


Figure 6: Sequence alignment of Osh proteins displaying ORD (red), OSBP fingerprint (yellow), PH domain (blue), GOLD domain (purple) and ankyrin-like repeats (orange) (19).

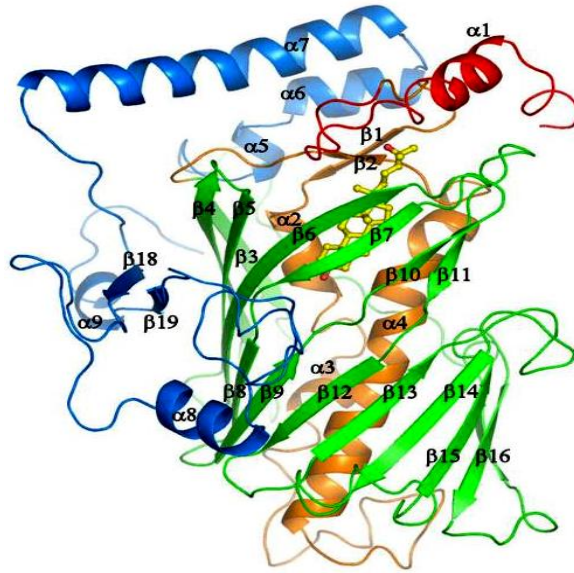


Figure 7: Ribbon protein structure of Osh4p/Kes1p displaying N-terminal lid (red), central helix (orange), C-terminal region (blue),  $\beta$ -barrel (green) and ergosterol (yellow) (21).

Osh4p does not have a specific phosphatidylinositol phosphate-binding domain (23). Studies have shown that ORPs, including Osh4p, can in fact bind to PIPs through ORD (24; 25). *In vitro* binding assays have shown that Osh4p is unable to distinguish PI(4)P from PI(4,5)P<sub>2</sub>-containing membranes (23; 26). Originally, sterol uptake by Osh4p was believed to be regulated by PI(4,5)P<sub>2</sub>, a plasma membrane (PM) lipid. However, this became hard to accept as genetic and cellular studies have shown that Osh4p has a specific role at the Golgi and that its sterol uptake was in fact regulated by PI(4)P, a Golgi lipid located on the trans side of the Golgi (25). The sterol/PI(4)P regulation became evident as a sterol/PI(4)P exchange pathway was proposed (Figure 8) (23).

The interaction of Osh4p with the anionic trans-Golgi membrane opens the lid of the ORD promoting the release of the sterol in exchange for a PI(4)P (Figure 8) (23). Consequently, Osh4p then transfers PI(4)P from the trans-Golgi to the ER where another

sterol will be extracted as an exchange, and the lipid/sterol exchange/transfer pathway continues for another round (Figure 8) (23). This cycle is proposed in parallel with the work of Sac1p/Pik1p and Sec14p. The phosphatase Sac1p dephosphorylates PI(4)P into PI and the kinase Pik1P phosphorylates PI into PI(4)P through the consumption of ATP (Figure 8) (23). The cycling of the lipids PI/PC between the ER and Golgi is done by the transfer protein Sec14p (Figure 8) (23). The human OSBP is believed to have a somewhat similar yet more complex PI(4)P/sterol exchange pathway.

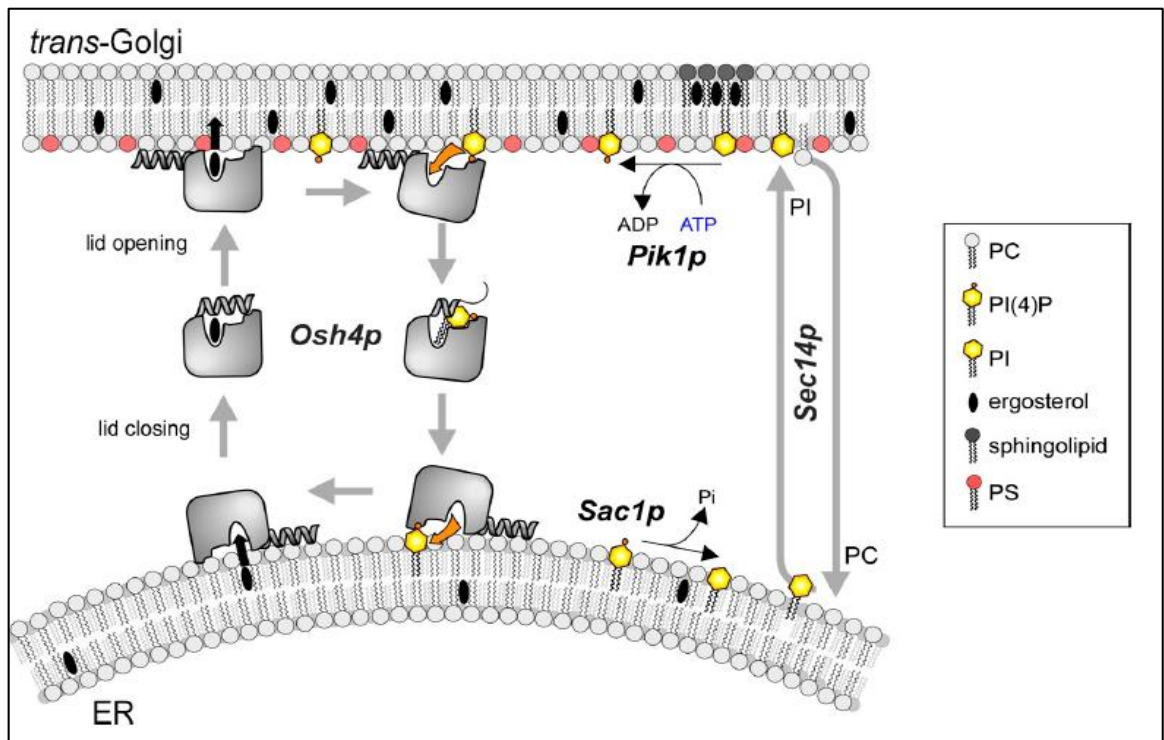


Figure 8: Proposed PI(4)P-sterol exchange pathway for the Osh4p (23). With an open lid, Osh4p picks up ergosterol from the ER membrane, closes its lid and transfers the sterol to the trans-Golgi membrane (23). At the trans-Golgi membrane, Osh4p exchanges ergosterol with PI(4)P where this lipid is transferred to the ER membrane and is exchanged for another ergosterol (23). This cycle is coupled with the dephosphorylation of PI(4)P into PI by Sac1p,

the phosphorylation of PI into PI(4)P through the consumption of ATP by Pik1p, and the exchange and transfer of PI and PC lipids by the protein Sec14p (23).

### **1.3.2. Oxysterol Binding Protein (OSBP)**

Human family members of ORPs are arranged into six subfamilies all of which possess the OSBP fingerprint sequence as well as the ORD (18). The majority of these proteins also possess a Pleckstrin Homology (PH) domain that plays a role in its binding and recognition of phosphatidylinositol-4-phosphates (PI(4)P) and a FFAT motif that binds to vesicle associated membrane protein (VAMP) VAP-A (Figure 9) (27; 18). OSBP (PI(4)P transporter) and other lipid transport proteins such as CERT (a ceramide transporter), FAPP2 (glucosylceramide transporter), Sec14 (phosphatidylinositol transporter) are found near the membrane contact sites (MCSs) between the Golgi and the ER (15; 20; 28; 29; 30). Except for Sec14, the previous mentioned proteins all share a common PH domain that helps recognize the Golgi membrane and a FFAT motif that helps recognize the ER membrane (31). Since OSBP contains PH and FFAT motifs, and can be located near the ER/Golgi, MCSs researchers have proposed that this protein tethers to both ER and Golgi during a proposed mechanism for sterol/PI(4)P exchange (Figure 10 and 11) (15).



Figure 9: Sequence alignment of human OSBP/ORP proteins displaying ORD (red), OSBP fingerprint (yellow), PH domain (green), ankyrin-like repeats (blue), VAP targeting motif (FFAT motif) (black) and trans-membrane domain (orange) (18). L and S represent long and short variants respectively (18).

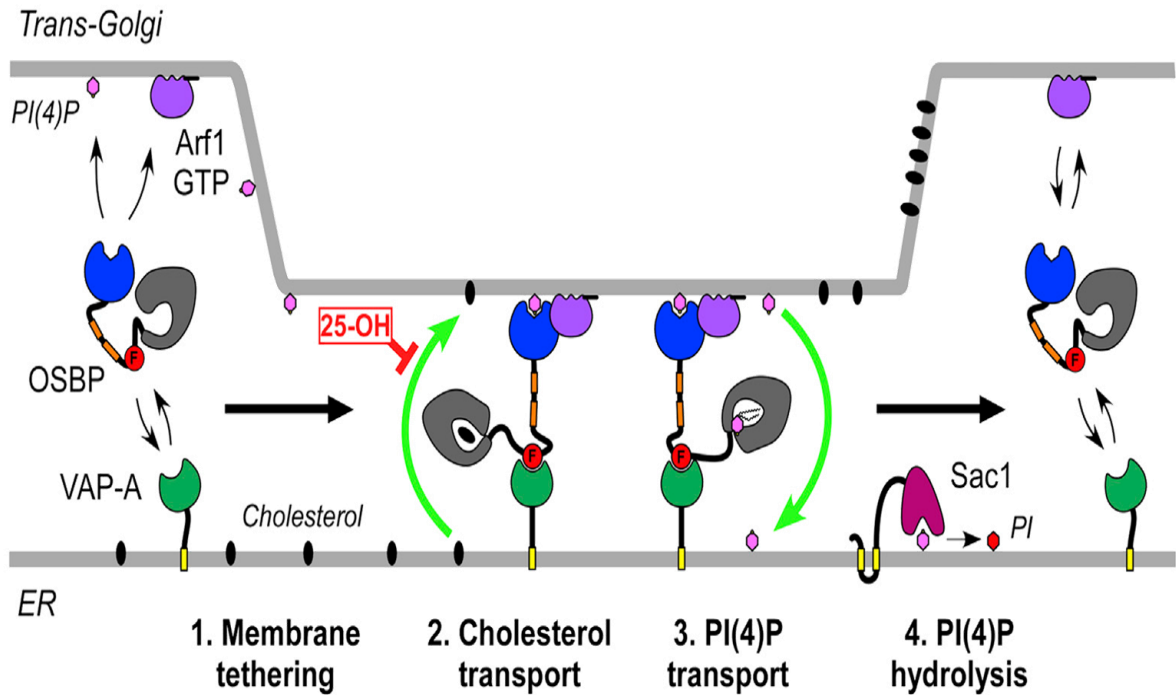


Figure 10: Proposed PI(4)P-sterol exchange pathway for the OSBP (15). Starting with membrane tethering, OSBP attaches itself to PI(4)P or ARF1-GTP by the PH domain and VAP-A by the FFAT motif. After OSBP tethers the ER/Golgi membranes, cholesterol is then extracted from the ER and transferred to the Golgi in which the sterol is exchanged with PI(4)P that is transferred to the ER. This proposed mechanism terminates when the PI(4)P that was transferred by OSBP is hydrolyzed by the phosphatase Sac1p. Lack of PI(4)P in the Golgi membranes would decrease membrane tethering and thus the rate of sterol transfer.

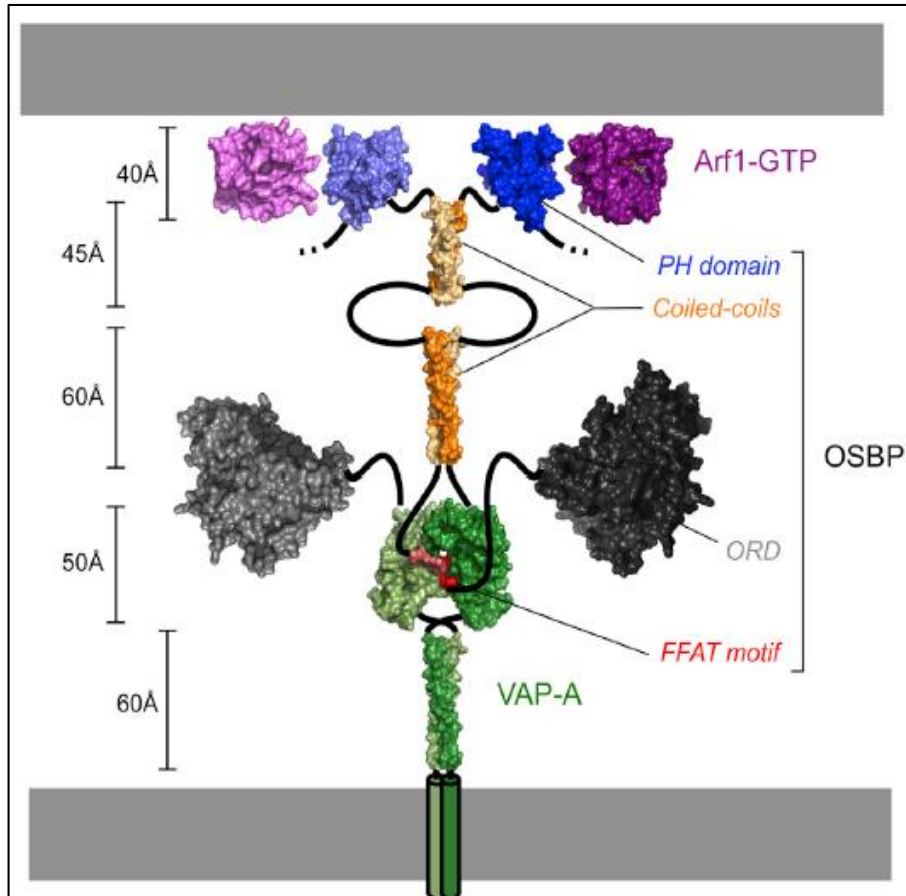


Figure 11: The organization of OSBP domains between the ER and Golgi (15). OSBP is suggested to form a dimeric rod-like structure as deduced from the domains of other related proteins: ORP11 PH domain (2D9X), Osh4p ORD domain (1ZHZ), VAP-A-FFAT motif complex (1Z9O), Arf1-GTP (1O3Y) and tropomyosin coiled-coil regions (2D3E). The tethering of OSBP to both the Golgi and ER membranes is done by the PH domain's attachment to ARF1-GTP and the FFAT motif's attachment to VAP-A (15).

The proposed PI(4)P/sterol exchange pathway for OSBP can be broken into four steps: membrane tethering, cholesterol transport, PI(4)P transport, and PI(4)P hydrolysis (Figure 10) (15). The rate limiting step of the PI(4)P/sterol exchange pathway is the hydrolysis of PI(4)P by Sac1p (15). This ensures that the pathway is irreversible and when

PI(4)P is limiting, the protein is signaled to end the tethering of the membranes (15). Membrane tethering is initiated upon the recognition of PI(4)P or ARF1-GTP by the PH domain and VAP-A by the FFAT motif of OSBP (15; 32; 33). OSBP is suggested to form a dimeric rod-like structure as deduced from the domains of other related proteins: ORP11 PH domain (2D9X), Osh4p ORD domain (1ZHZ), VAP-A-FFAT motif complex (1Z9O), Arf1-GTP (1O3Y) and tropomyosin coiled-coil regions (2D3E) (Figure 11) (15). After OSBP tethers the ER/Golgi membranes, cholesterol is then extracted from the ER and transferred to the Golgi. OSBP's ability to transfer sterols has been debated as Osh/ORP proteins have not been able to transfer sterols fast enough to account for the quick redistribution of cholesterol between organelles (34). However, Mesmin *et al.* were able to show a “maximal turnover rate of  $0.5 \text{ s}^{-1}$ , or 30 dehydroergosterols (DHE) transferred per OSBP per minute” (15). After the transfer of cholesterol from the ER to the Golgi by OSBP, OSBP exchanges cholesterol for a PI(4)P. Such an exchange was evident with Osh4p (23). This proposed mechanism terminates when the PI(4)P that was transferred by OSBP is hydrolyzed by the phosphatase Sac1p. Lack of PI(4)P in the Golgi membranes would decrease membrane tethering and thus the rate of sterol transfer. However, details about the rates of the hydrolysis of PI(4)P by Sac1p are still under investigation. Sac1p was originally shown to hydrolyze PI(4)P in *trans*-Golgi, which meant that (based on the proposed hypothesis) OSBP will have to competitively bind to PI(4)P with Sac1p; but the current proposed pathway can only be effective if the Sac1p works in *cis*-Golgi or if Sac1p cycles between ER and Golgi, as OSBP transfers PI(4)P from *trans* to *cis* membrane (35). Mesmin *et al.* have argued that by positioning the Sac1p at the *trans* location, the cellular distribution of PI(4)P is not affected nor does it promote the hydrolysis of PI(4)P (15). Furthermore,

Mesmin *et al.* have demonstrated that Sac1p works in *cis* location reinforcing their current proposed lipid/sterol exchange/transfer OSBP pathway (15). Aside from the proposed sterol exchange/transfer OSBP pathway, OSBP is also subject to phosphorylation which may also control the directionality of its activity.

#### **1.4. Protein Phosphorylation**

Many proteins undergo post-translational phosphorylation through the action of protein kinases at the consumption of ATP (36). Removal of the phosphate group is accomplished by phosphatase enzymes (36). In order to phosphorylate a protein, the amino acids serine, threonine, tyrosine, histidine, arginine and lysine residues are targeted (37). Kinases share a catalytic domain that catalyze the transfer of the gamma-phosphate of ATP to one of the targeted amino acid residues such as serine (38). Protein kinases are regulated by various mechanisms including but not limited to the control of their phosphorylation state (38). In addition, protein phosphorylation plays multiple roles in signalling pathways and cellular processes, many of which are regulatory processes (36). For example, in the first step of glycolysis and in order to initiate glycolysis, glucose is phosphorylated by hexokinase to form glucose-6-phosphate (G6P) at the consumption of ATP (39). This can be reversed by the enzyme glucose-6-phosphatase in which G6P is hydrolyzed to glucose and orthophosphate (39).

Returning to the topic of phosphorylation of OSBP, the phosphorylation cycle of OSBP has been linked to Golgi localization and the cholesterol/SM (sphingomyelin) content of cells (1). Although the ER is the location of where cholesterol is synthesized, the rapid transfer of cholesterol to the Golgi makes the ER a cholesterol-poor environment. Since the

ER is poor in cholesterol compared to the Golgi, OSBP needs a mechanism that allows it to deliver cholesterol against a concentration gradient, hence OSBP undergoes a rapid phosphorylation cycle that is linked to Golgi localization and the cholesterol content in the ER (27; 40). Therefore, depletion of cholesterol at the ER causes OSBP dephosphorylation and Golgi localization (27; 40).

In order to better understand the effect of the phosphorylation cycle on OSBP's transfer/exchange activity, Goto *et al.* designed OSBP phosphomutants in order to study their effects on the transfer/exchange OSBP pathway (27). OSBP has two sites in which serine repeats can be phosphorylated (Figure 12) (27). The serine (S) to glutamic acid (E) mutation is to mimic the phosphorylation at these sites by installing permanently anionic glutamate groups (Figure 13) (27). Focusing primarily on the phosphomimic OSBP-S5E, in which five serine residues were mutated to glutamic acid residues, Goto *et al.* demonstrated that this mutant has increased sterol binding capacity, higher cholesterol extraction, but reduced transfer activity and the binding of PI(4)P was not affected (27). Better understanding the work of this mutant can help fully understand the phosphorylation cycle of OSBP to the OSBP sterol/lipid transfer/exchange pathway.

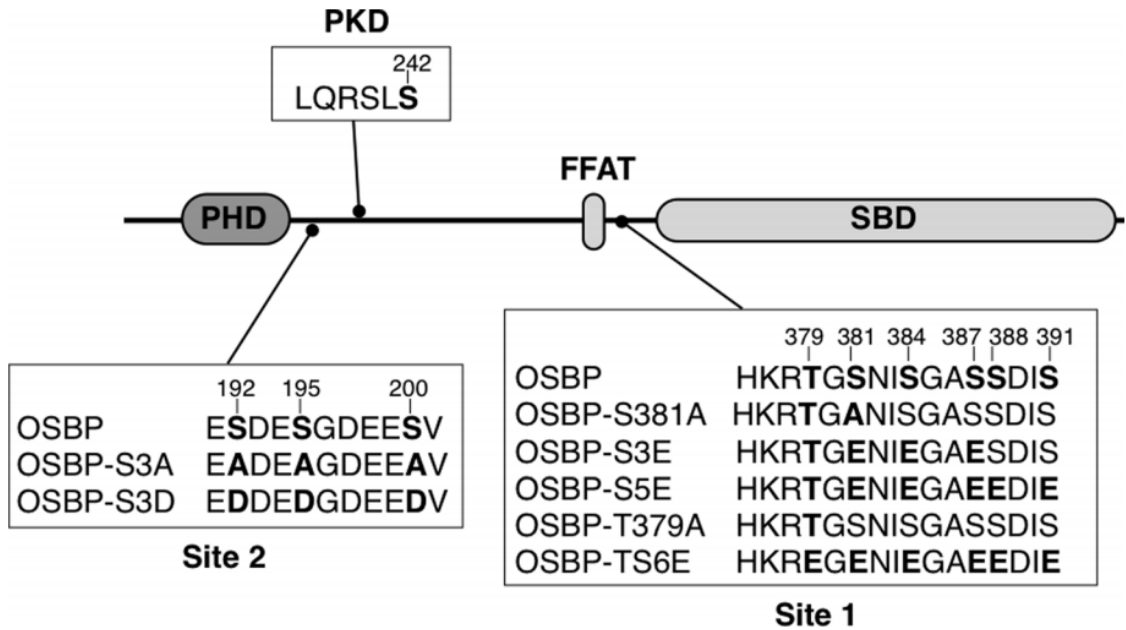


Figure 12: Mutations at different phosphorylation sites of OSBP (27). OSBP has two possible sites of phosphorylation. In order to mimic the properties of the phosphorylation state of OSBP, glutamic acid (E) residues replaced serine (S) residues; such was the case in OSBP-S5E where 5 serine residues were replaced by glutamic acid residues.

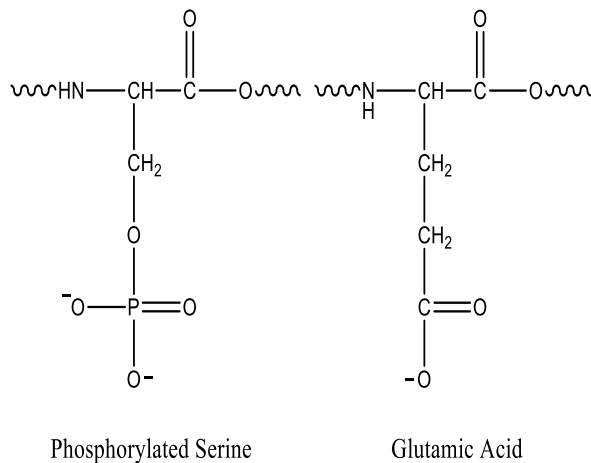


Figure 13: The chemical structure of phosphorylated serine in comparison to glutamic acid (27). Glutamic acid residues were used to mimic the anionic properties of the

phosphorylated serine residues. This was used in the design of OSBP-S5E mutant in which 5 serine residues were mutated to glutamic acid residues (27).

### **1.5. Overview of Project**

The objective of this thesis is to examine the role of OSBP phosphorylation on sterol/lipid binding and extraction. Phosphorylation of OSBP has been linked to OSBP's localization to the Golgi and the cholesterol/SM content of the cells. Depletion of cholesterol, by inhibition, at the ER results in dephosphorylation of OSBP and Golgi localization (27; 40). OSBP's localization to the Golgi may be part of the current OSBP proposed pathway (15). The phosphorylation cycle of OSBP is showing potential as a means of control in the directionality and/or specificity of the transfer activity.

The role of OSBP phosphorylation will be studied via protein-lipid binding assays and fluorescent based assays. The protein-lipid binding assays will be examined through dual polarization interferometry (DPI). DPI is an analytical technique capable of measuring protein adsorption to phospholipid bilayers that are immobilized on a silicon oxynitride sensor surface (41). Small unilamellar vesicles (SUVs) mimicking the Golgi/ER membranes will be constructed and used. SUVs will include a high concentration of the DOPC lipid with/without variable concentrations of the phospholipid PI(4)P or the sterols cholesterol and 25-hydroxycholesterol. Using DPI, the real-time behavior of the binding kinetics of OSBP to different compositions of lipid membranes will be examined.

In addition, the role of OSBP phosphorylation will be examined through fluorescence binding assays. The ability of OSBP to bind cholesterol will be studied using the cholesterol analogue 22-NBD-cholesterol through a fluorescence based binding assay.

The ultimate goal of this thesis is to evaluate the role of OSBP phosphorylation on sterol/phospholipid binding. The binding kinetics of OSBP-S5E with sterol/PI(4)P containing membranes will be analyzed in comparison to wt-OSBP.

## 2. MATERIALS AND METHODS

### 2.1. Consumable Products

50 mL Falcon tubes

Amicon Ultra Centrifugal Filters (Ultracel – 50K)

AnaLight Bio 200 FB80 chips

Avestin Polycarbonate Membrane – 100 nm

Bio-Rad Macro-Prep DEAE Support Weak Anion Exchange Support

T-25 flasks

### 2.2. Chemical Reagents and Solutions

#### 2.2.1. Enzymes, Antibiotics and Lipids

10,000 U/mL Penicillin-Streptomycin (Life Technologies/ThermoFisher Scientific, Burlington)

25-OH Cholesterol (Oxysterol) (Avanti Polar Lipids, Alabama)

Cholesterol (Avanti Polar Lipids, Alabama)

Complete Tablets Mini EDTA-free *EASYpack* – protease inhibitor cocktail tablets (Roche, Sigma-Aldrich Co., Canada)

DOPC (1,2-dioleoyl-sn-glycero-3-phosphocholine) (Avanti Polar Lipids, Alabama)

Fungizone Antimycotic (Amphotericin B) (Life Technologies/ThermoFisher Scientific, Burlington)

NBD-Cholesterol (22-(*N*-(7-Nitrobenz-2-Oxa-1,3-Diazol-4-yl)Amino)-23,24-Bisnor-5-Cholen-3 $\beta$ -Ol) (Avanti Polar Lipids, Alabama)

PI(4)P (phosphatidylinositol-4-phosphate) (Avanti Polar Lipids, Alabama)

### **2.2.2. Baculovirus and Insect Cells**

OSBP-wt Baculovirus liquid sample with measured titre was supplied by Dr. Neale Ridgway, Dalhousie University, Halifax, NS. Stored at 4°C away from light.

OSBP-S5E Baculovirus liquid sample with measured titre was supplied by Dr. Neale Ridgway, Dalhousie University, Halifax, NS. Stored at 4°C away from light.

The insect cell line Sf21 Cells (*Spodoptera frugiperda* line 21) (Life Technologies/ThermoFisher Scientific, Burlington): 1 x 10<sup>7</sup> cells in 1 mL Sf-900 III SFM.

### **2.2.3. Culture Medium and Buffers**

#### **2.2.3.1. Culture Medium**

Insect cell culture medium contains (~1 L):

1 L Sf-900 III SFM (*Spodoptera frugiperda* 900 III serum free medium - liquid) (Life Technologies/ThermoFisher Scientific, Burlington)

5% (50 mL) Fetal Bovine Serum (Life Technologies/ThermoFisher Scientific, Burlington)

100 U/mL (10 mL of 10,000 U/mL stock) Penicillin-Streptomycin (Life Technologies/ThermoFisher Scientific, Burlington)

0.25 µg/mL (1 mL) Fungizone Antimycotic (Amphotericin B) (Life Technologies/ThermoFisher Scientific, Burlington)

#### **2.2.3.2. OSBP Purification Buffers**

Buffer A (wash buffer): 50 mM NaH<sub>2</sub>PO<sub>4</sub>, 300 mM NaCl, pH 7.4

Buffer B (elution buffer): 50 mM NaH<sub>2</sub>PO<sub>4</sub>, 300 mM NaCl, 250 mM Imidazole, pH 7.4

Cleaning buffer 1: 1% CH<sub>3</sub>COOH, 1% H<sub>3</sub>PO<sub>4</sub>

Or 70% EtOH

Or 30% IPA

Cleaning buffer 2: 20 mM NaH<sub>2</sub>PO<sub>4</sub>, 1 M NaCl, 0.1 M EDTA, pH 7.4

Cobalt solution: 0.2 – 0.3 M CoCl<sub>2</sub>·6H<sub>2</sub>O

Lysis buffer: 20 mM Tris-HCl, 150 mM NaCl, 1% Triton X-100, pH 7.4

Sodium acetate buffer: 50 mM CH<sub>3</sub>COONa, pH 4.0

Storage buffer: 20% EtOH

#### **2.2.3.3. Sodium Dodecyl Sulphate (SDS) Polacrylamide Gel Electrophoresis Buffers**

40% Acrylamide/Bis-Acrylamide Solution (Bio-Rad, Toronto)

SDS-PAGE Separating Buffer: 1.5 M Tris-HCl, pH 8.8

SDS-PAGE Stacking Buffer: 0.5 M Tris-HCl, pH 6.8

6x SDS-PAGE Loading Dye: 0.6 M dithiothreitol (DTT), 350 mM Tris-HCl, 30% glycerol, 10% SDS, 0.12% bromophenol blue, pH 6.8

10x SDS-PAGE Running Buffer: 250 mM Tris-Cl, 1.92 M glycine, 1% SDS, pH 8.3

ProtoBlue Safe staining solution (Colloidal Coomassie G-250 Stain) (National Diagnostics, Atlanta, GA, USA)

Pre-stained Broad Range Protein Ladder (New England BioLabs, Ipswich, MA, USA)

#### **2.2.3.4. Ion Exchange Chromatography Buffer**

Running buffer (RB): 50 mM Tris, pH 8.5

Salt buffer (SB): 50 mM Tris, 500 mM NaCl, pH 8.5

#### **2.2.3.5. Dual Polarization Interferometry (DPI) Buffer**

DPI buffer: 10 mM K<sub>2</sub>HPO<sub>4</sub>, 137 mM NaCl, pH 7.4

#### **2.2.3.6. Fluorescent Based Assay Buffers**

DPI buffer, same as previously mentioned

### **2.3. Equipment and Programs**

*AnaLight Bio 200*

AnaLight Explorer Inject software

AnaLight Explorer software

Avanti Polar Lipids extrusion apparatus/Hamilton Gastight #1001

Beckman Coulter Allegra X-30R Centrifuge – SX4400 Rotor

Bio-Rad BioLogic DuoFlow

Bio-Rad Gel Doc Ez Imager

Bio-Rad Image Lab software

Bio-Rad – Mini-Protean III apparatus

Farfield AnaLight Bio 200

Fisher Scientific Isotemp incubator

Harvard Apparatus PHD 2000 Programmable Pump

New Brunswick Scientific Co. Incubator Shaker – Series I26

New Brunswick Scientific Co. Incubator Shaker – Series 25

Photon Technology International (PTI) Fluorometer

Photon Technology International (PTI) software

QSonica Sonicators

SterilGARD Hood – the Baker Company, Inc. (biological safety cabinet)

Thermo Scientific Sorvall Centrifuge – SS-34 Rotor

Zeiss microscope

## **2.4. Experimental Protocols**

### **2.4.1. Growth of Sf21 Cells**

Commercially supplied frozen stocks of Sf21 cells (1 mL,  $1 \times 10^8$  cells/mL) were thawed on ice. Prior to complete thawing of cells, the cells were transferred to a T-25 flask. The cell culture was left for 15 minutes to let the cells settle and form a monolayer adherent to the flask. The flask was turned to an upright position in which the liquid medium and floating cells were discarded, and 2 mL of fresh culture medium (pre-heated at 37°C) was added. The monolayer cell culture was then placed in an aerated sterile incubator set to 28°C.

Monolayer cultures were grown for 3-4 days until they became 80-90% confluent. At this stage, the monolayer culture was sub-cultured in a biosafety cabinet. Without shaking the flask, the Sf21 monolayer culture was transferred into the biosafety cabinet hood. While in an upright position, the culture medium including the floating cells was transferred into the waste tube. Two milliliters of new culture medium (pre-heated at 37°C) was added into the monolayer culture and the flask was closed. The flask was then tapped hard on its sides to dislodge the cells. At times, since the cells do attach very tightly, it was necessary to shake the flask vigorously. 0.5 mL of the culture was transferred into a sterile 1 mL microfuge tube and the cell density and viability were determined using a hemocytometer and 0.4% trypan blue solution. Another 0.5 mL of the culture was then transferred into a new T-25 flask followed by an addition of 1.5 mL culture medium to it. The last 1 mL of culture was transferred to waste.

After a minimum of two monolayer generations have passed, the 1 mL culture that is usually transferred to waste is now transferred to a 250 mL Erlenmyer flask, followed by addition of 24 mL of culture medium (pre-heated to 37°C). This culture was put into a shaker incubator (New Brunswick Scientific Co. Incubator Shaker Series 25) set to 28°C and 140-160 rpm. The suspension culture was then left to grow for another 4-5 days. The cell density and viability was then determined using a hemocytometer and 0.4% trypan blue solution. The suspension culture was then sub-cultured to a 1 L Erlenmyer flask containing ~250 mL culture medium (pre-heated at 37°C) in which 5-10 mL of the culture was transferred using a Pasteur pipette in the biosafety cabinet. The new suspension culture was left to grow in a shaker incubator (New Brunswick Scientific Co. Incubator Shaker Series 25) set to 28°C and 140-160 rpm for 4 days. Following the growth of the cells, the cell density and viability was then determined using a hemocytometer and 0.4% trypan blue solution. If the cell density is between  $1 \times 10^6$  to  $2 \times 10^6$  cells/mL, the cells were determined to be ready for infection. If the cell density was lower than that, the suspension culture was left to grow for another day, or sub-cultured into a new flask for a new suspension culture.

#### **2.4.2. Preparation of Sf21 Freeze Stock Cultures**

After a minimum of 5 monolayer culture generations have passed with a healthy and similar pattern of growth, the 1 mL culture that was transferred to waste or culture medium to start a suspension sub-culture was now transferred to a 1 mL cryovial to prepare a freeze stock culture. DMSO was added to a final concentration of 10%. The cryovial was stored for preservation at either -80°C or liquid nitrogen.

### **2.4.3. Baculovirus Infection of Sf21 Cells (Expression of OSBP and Baculovirus)**

After the suspension culture reached an appropriate cell density between  $1 \times 10^6$  cells/mL and  $2 \times 10^6$  cells/mL, a total of  $1.8 \times 10^6$  cells were transferred to a Falcon tube. The cells were centrifuged at  $4000 \times g$  using Rotor Beckman Coulter Allegra X-30R Centrifuge – SX4400 Rotor for 5 minutes and the medium was transferred to waste. OSBP construct-containing baculovirus was added to an MOI of 1.5 and the volume was brought up to 25 mL using culture medium (pre-heated to  $28^\circ\text{C}$ ). The infected cells were covered with tin foil and thoroughly mixed using a bench top rotator for one hour. After that, the cells were transferred to a 1 L Erlenmeyer flask containing 225 mL of culture medium (pre-heated at  $28^\circ\text{C}$ ). The flask was transferred to a shaker incubator (New Brunswick Scientific Co. Incubator Shaker Series 25) set to  $28^\circ\text{C}$  and 140-160 rpm for 3-4 days, which the cells were observed under a microscope and monitored daily for an increase in the cell diameter size. Once the diameter of the cells increased to 1.5 – 2 times the original size, the cells were then pelleted at  $4000 \times g$  using the Beckman Coulter Allegra X-30R Centrifuge – SX4400 Rotor for 5 minutes. The supernatant was saved and filtered for use as baculovirus in which its titre was determined using plaque assays, a technique that counts the number of plaque forming units on Sf21 baculovirus-infected cells plugged with agar. The pellets were stored at  $-80^\circ\text{C}$ .

### **2.4.4. Preparation of Resin for Column Chromatography**

20 mL of immobilized-metal affinity chromatography (IMAC) uncharged resin was transferred to a 50 mL Falcon tube and spun at  $4000 \times g$  for 5 minutes using the Beckman Coulter Allegra X-30R Centrifuge – SX4400 Rotor. The ethanol supernatant was discarded

and 40 mL of sodium acetate buffer (50 mM) was added. The resin was shaken vigorously, spun on a rotator for few minutes until the resin was thoroughly mixed. The resin was centrifuged at 4000 x g for 5 minutes and the supernatant was discarded. The sodium acetate buffer was added again and the steps were repeated for 2 more cycles. 40 mL of 0.2-0.3 M cobalt solution ( $\text{CoCl}_2 \cdot 6\text{H}_2\text{O}$ ) was added to the resin and the resin was left to mix on a bench rotator for overnight.

The cobalt-charged resin suspension was centrifuged at 4000 x g for 5 minutes and the supernatant was discarded. 40 mL of sodium acetate buffer was added to the resin, mixed thoroughly then centrifuged at 4000 x g for 5 minutes. This step was repeated two more times, followed by 3 similar washes with distilled water and 2 washes with lysis buffer. 40 mL of lysis buffer was then added and the resin was left to mix overnight on a rotator placed inside a 4°C environment.

#### **2.4.5. Purification of OSBP**

A frozen pellet (~5 mL volume, ~2 g mass of wet cells) of Sf21 cells was taken out and left to thaw on ice. 20 mL of lysis buffer and 1 tablet of protease inhibitor (complete Tablets Mini EDTA-free *EASYpack*) were added to the pellet. Using a pipette, the pellet and the tablet were thoroughly broken in the lysis buffer. The mixture sat on ice for a 30 minute incubation period. The lysed cells were further broken by passing them through 18 gauge and 23 gauge needles for a minimum of 5 times. The lysed cells were then sonicated using a probe sonicator (QSonica Sonicators) for 1 minute set to 5 sec/pulse. 5-10  $\mu\text{L}$  of DNase (10,000 units) was then added and the mixture sat on ice for another 30 minute incubation period.

The lysed cells were then transferred to a SS-34 Sorvall tube and centrifuged at 40,000 x g for 45 minutes using the Thermo Scientific Sorvall Centrifuge – SS-34 Rotor. In the meantime, the resin-lysis buffer mixture was split into two 50 mL Falcon tubes and spun for 5 minutes at 4,000 x g. The supernatant of the resin was discarded, and the supernatant of the cells was added to the resin. The resin-lysed cells mixture was left to thoroughly mix on a rotator overnight in a 4°C environment.

The incubated resin was transferred to a Bio-Rad glass column. Using gravity, the resin mixture was passed through the column enabling the resin to settle with a minimal layer of liquid on top. The glass column was then set up on its holding apparatus and transferred to a fast protein liquid chromatography (FPLC) machine (Bio-Rad BioLogic DuoFlow) for an automated purification procedure.

Prior to purification, the FPLC (Bio-Rad BioLogic DuoFlow) was washed using ethanol, water and purification wash buffer (Buffer A). The column was then set up on the FPLC machine and the automated purification protocol was started. The FPLC was set to pass 40 mL of purification wash buffer (100% Buffer A) at 4 mL/min, followed by 40 mL of low imidazole (20 mM) wash buffer (92% Buffer A, 8% Buffer B) at 4 mL/min and 40 mL of high imidazole (200 mM) wash (elution) buffer (20% Buffer A, 80% Buffer B) at 4 mL/min. Flow-through of the low and high imidazole washes were collected for analysis. The FPLC machine was set to monitor protein elution at UV/Vis absorbance of 280 nm. During the initial stages of the high imidazole wash, a small peak in absorbance was observed indicating the presence of the protein. The column was then washed using MES buffer before removal from the FLPC and storage.

After the purification of OSBP was complete, the resin was subjected to the removal of its metal ions using sodium phosphate buffer (Cleaning buffer 2), cleaning using acetic acid/phosphoric acid buffer (Cleaning buffer 1) with an exposure of 10 – 15 minutes, and recharged as per previously discussed.

#### **2.4.6. Protein Quantification**

Quantification of protein was performed using the Bradford assay method and the Bradford reagent (BioShops). Bovine serum albumin (BSA), concentrations from 10 µg/mL to 1000 µg/mL were prepared in 50 µL total volume in PBS buffer and added to 1 mL Bradford reagent in 1.5 mL plastic cuvettes. The absorbance of the samples were measured at 595 nm and through interpretation, a linear regression model of the standard curve was determined. 50 µL of potential protein sample was added to 1 mL Bradford reagent in 1.5 mL cuvette had its absorbance measured at 595 nm. Using the absorbance value and equation of the regression line analysis, the protein concentration was calculated.

#### **2.4.7. SDS-PAGE Electrophoresis**

Samples collected including supernatant, washes and protein were analyzed for purity using SDS-PAGE. The SDS-PAGE gels were commercially supplied or self-made using recipes shown in Table 1.

Table 1: SDS-PAGE gel recipe of 12% separating gel and 4% stacking gel for 6 gels.

	12% Separating Gel	4% Stacking Gel
Distilled Water	20.5 mL	18.8 mL
Stacking Buffer	-	7.5 mL
Separating Buffer	12.0 mL	-
40% Acrylamide/Bis-Acrylamide	14.4 mL	3.0 mL
10% SDS	480 $\mu$ L	300 $\mu$ L
50% Glycerol	100 $\mu$ L	74 $\mu$ L
TEMED*	48 $\mu$ L	30 $\mu$ L
10% APS*	480 $\mu$ L	300 $\mu$ L

\*TEMED and APS were added at the end, right before pouring into apparatus.

The Mini-PROTEAN III (Bio-Rad) gel castings were assembled according to manufacturer's instructions. The 12% separating gel formula was poured into the gel castings and left to polymerize for 30 minutes to 1 hour with an overlaid layer of iso-propanol. After polymerization, the iso-propanol was poured out and completely removed using a kim-wipe. The stacking gel formula was then poured on top of the separating gel, followed by the addition of the comb and left to polymerize for a minimum of 30 minutes. The gel was then covered with paper towels hydrated with distilled water and stored at 4°C overnight.

Prior to SDS-PAGE, the comb of the gel was removed and the gel castings were set up on the Bio-Rad SDS-PAGE apparatus. SDS-PAGE buffer was poured in the middle of

the apparatus to let the bubbles escape. Up to 25  $\mu\text{L}$  of to-be-analyzed samples ( $\sim 2$   $\mu\text{g}$  of protein) were each mixed with up to 5  $\mu\text{L}$  of 6x SDS-PAGE loading buffer and denatured in a water bath set to  $95^{\circ}\text{C}$  for 5 minutes. Each sample was loaded into a separate well, and alongside the protein samples, 8  $\mu\text{L}$  of commercially supplied pre-stained broad range protein marker was loaded. The gel was then ran at 120 V for 1.75 hours.

Prior to analysis, the protein gel was stained for a minimal of 6 hours in a staining solution (10% ProtoBlue and 90% EtOH), followed by destaining with distilled water for overnight. During the use of the commercially supplied stain-free gels (BioRad), the staining protocol was exempted. Using the Bio-Rad Gel Doc Ez Imager, a gel picture was obtained under white light and then was analyzed using Bio-Rad Image Lab software.

#### **2.4.8. Buffer Exchange**

The commercially supplied buffer exchange column was set up, and exchange buffer in the column was left to drain out. 10 mL of the buffer of interest (commonly DPI buffer) was added and left to flow through. 3 mL of protein sample was added and left to flow through. 4 mL of the buffer of interest (commonly DPI buffer) was added and collected in 5 mL culture tubes. The addition of protein sample and buffer of interest steps were repeated until all the protein samples have passed through. The column was then washed with a minimal of 10 mL of PBS buffer. The column was then filled back up with PBS buffer + minimal sodium azide mixture (0.02%) before storing on bench top. Upon the completion of buffer exchange, the protein samples are concentrated using Amicon Ultra Centrifugal Filters Ultracel – 50K (spun at  $4000 \times g$  using Beckman Coulter Allegra X-30R Centrifuge

– SX4400 rotor for 8 minutes) and re-quantified using Bradford assay as previously discussed.

#### **2.4.9. Ion-Exchange Chromatography**

3 mL of commercially supplied DEAE Sepharose resin (Bio-Rad Macro-Prep DEAE Support Weak Anion Exchange Support) was prepared as per company protocol (removed storage buffer, equilibrated in running buffer, added protein, set up column apparatus and transferred to FPLC machine (Bio-Rad BioLogic DuoFlow) for an automated protocol). 50 mL of low salt wash buffer (90% running buffer (RB), 10% salt buffer (SB)) was then passed through followed by 20 mL of medium salt wash buffer (50% RB, 50% SB) and then 30 mL of high salt wash buffer (100% SB). The flow rate was set to 1 mL/min and all eluted samples of 3 mL aliquots were collected and analyzed for purity.

#### **2.4.10. Unilamellar Vesicle Preparation**

##### **2.4.10.1. Large Unilamellar Vesicle Preparation (DPI Lipids)**

Lipids (Avanti Polar Lipids) were aliquoted to appropriate compositions in glass vials. The total volume of the lipids was prepared in sets of 2 mL and was based on the test the lipids were to be used for; e.g. DPI lipid binding assay. The chloroform solvent of the lipid compositions was evaporated using nitrogen gas, followed by a mechanical vacuum pump for 45 minutes to 1 hour. The lipids were then hydrated with the appropriate amount of buffer appropriate for the test the lipids were to be used for (e.g. DPI buffer for DPI lipid-binding assay). The hydrated lipids were lightly vortexed, then left overnight in a 4°C environment.

Prior to their use, the lipids were lightly vortexed again and were extruded using Avanti Polar Lipids extrusion apparatus/Hamilton Gastight #1001 using 100 nm filters (Avestin Polycarbonate Membrane – 100 nm). The lipids were passed through the filter 15 times. Extruded lipids were used immediately or within 24 hours of their extrusion.

#### **2.4.11. Dual Polarization Interferometry – Membrane Lipid-Protein Binding Assay**

The DPI machine (Farfield *AnaLight Bio 200*) protocol was a modification to the protocol provided by Farfield Scientific Ltd. After the machine (Farfield *AnaLight Bio 200*) and pump (Harvard Apparatus PHD 2000 Programmable Pump) were turned on and the lamp was left to warm up, air was injected into the machine multiple times ensuring minimal amount of liquid remained in the tubes of the machine. The chip holder was then taken out, and the chip (*AnaLight Bio 200 FB80*) and its silicon cover were then cleaned using 2% Hellmanex, 10% SDS, 50% isopropanol (IPA), 80% EtOH and finally distilled water. In cases of difficult to handle chips (difficult to obtain clean fringes), distilled acetone was used as well. The chip holder was set back into the machine and DPI buffer was flowed through the machine using the external pump set to 100-250  $\mu\text{L}/\text{min}$ . 0.8 mL of 50% IPA was then injected and flowed through using the pump setting of 100  $\mu\text{L}/\text{min}$ . It is important to note that every injection performed was done with a minimal volume of 0.7 mL in which a total of 200  $\mu\text{L}$  is passed through each channel. In addition, the flow rate was controlled via the external pump (Harvard Apparatus PHD 2000 Programmable Pump), and the injection was commanded via the DPI injection software (*AnaLight Explorer Inject software*) on the connected computer. The DPI machine software (*AnaLight Bio 200*) was then opened, and the channels of the chip were examined for the best possible selection of fringes, a section within an observational window of the interference pattern that was produced from the light

shining through the sensing waveguide and reference waveguide. Upon successful selection of fringes, the machine was considered ready for protein-lipid binding assays.

Protein-lipid binding assays began after calibration of DPI machine (Farfield *AnaLight Bio 200*) using EtOH and distilled water. Leaving the window open (DPI injection software [*AnaLight Explorer Inject* software] program set to 1  $\mu\text{L}/\text{min}$ ), 80% EtOH was injected at flow rate of 100  $\mu\text{L}/\text{min}$  (pump flow rate) for exactly 1 minute and 30 seconds then changed to a 15  $\mu\text{L}/\text{min}$  flow rate (pump flow rate). The real-time examined signal dropped, after a sharp increase, to a flat line as the EtOH was completely passed through the channels. The injection channel window was then reset and all subsequent injections were made to a program injection flow rate equal to the pump (Harvard Apparatus PHD 2000 Programmable Pump) flow rate. Distilled water was then injected at a flow rate of 50  $\mu\text{L}/\text{min}$  and the calibration process was completed.

Protein-lipid DPI binding assays began with an injection of the lipid of interest (e.g. 0.5 mM 100% DOPC) at a flow rate of 25  $\mu\text{L}/\text{min}$  followed by a DPI buffer injection set at 50  $\mu\text{L}/\text{min}$ . The protein of interest (e.g. 1.0  $\mu\text{M}$  of wt-OSBP) was then injected at a flow rate of 25  $\mu\text{L}/\text{min}$ . The protein injection was monitored beyond its injection period up until no change in signal can be observed. The chip was then cleaned and reset for another protein-lipid binding test using injections of 2% Hellmanex, 10% SDS, 50% IPA, 80% EtOH, distilled water and DPI buffer set to a flow rate of 50  $\mu\text{L}/\text{min}$  or 100  $\mu\text{L}/\text{min}$ .

Data produced via the DPI machine software was saved and analyzed through the DPI analysis software (*AnaLight Explorer* software) using the protocol provided by Farfield Scientific Inc.

## **2.4.12. Fluorescent Based Assays**

### **2.4.12.1. Binding Assay**

The Photon Technology International (PTI) fluorometer was turned on and the xenon lamp was ignited and left to warm up to a setting of ~140 W. Test samples were made to a composition of 0.2  $\mu$ M protein of interest (e.g. wt-OSBP) and DPI buffer to a total volume of 1 mL in quartz cuvettes. The fluorometer was set with a slit width of 6 nm, and an emission and excitation wavelengths based on the fluorescent ligand of interest (e.g. excitation of 469 nm and emission of 537 nm for 22-NBD-cholesterol). The window in which the fluorescence of the ligand was monitored was set to the suggested minimal  $\pm$  10 nm of the emission wavelength (e.g. 527-547 nm in the case of 22-NBD-cholesterol). A background fluorescence value was obtained for each of the samples prior to the addition of fluorescent ligand. Volume of 0.5-1.0  $\mu$ L of fluorescent ligand (e.g. 22-NBD-cholesterol) from different stocks was added to each sample. The samples were then incubated for 8 minutes while mixing end over end using a bench top rotator. Each sample was subsequently measured and the fluorescent values were recorded.

### 3. RESULTS AND DISCUSSION

#### 3.1. Growth of Sf21 Cells

Prior to the start of this thesis, the Sf21 cells were grown using a similar protocol to the one previously outlined (section 2.4.1) with the exception of T-75 flasks instead of T-25 and different volumes. The previous protocol was initiated by my colleague Parthajit Mukherjee, in which the total flask volume was 20 mL (1 mL of initial stock of cells, 19 mL of culture medium). Instead of the 0.5/0.5/1 mL volumes in the T-25 protocol, the volumes were 1/1/3 mL. For the suspension culture, instead of the initial 1 mL to 24 mL of medium, 3 mL to 47 mL of medium was used instead. The cell growth pattern, cell density, remained quite similar for both protocols and prior to subculture, the monolayer cultures had an average cell density between  $2 \times 10^6$  cells/mL and  $8 \times 10^6$  cells/mL with an average cell viability between 95-99%. The protocol was adjusted to use T-25 flasks instead of T-75 flasks in order to save cost on material and medium. The growth of the cells was monitored and observed under a microscope. Figure 14 displays Sf21 monolayer culture at different magnifications after sub-culturing (Day 0). Figure 15 displays Sf21 monolayer culture after 2 days of growth with different magnifications. Figure 16 displays Sf21 monolayer culture at different magnifications prior to being sub-cultured (Day 4).

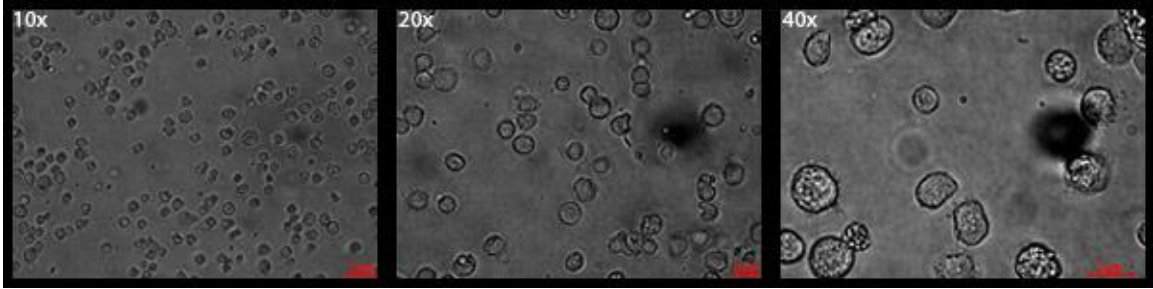


Figure 14: Sf21 monolayer culture after sub-culturing (Day 0) under different magnifications (10×, 20× and 40× respectively). The red lines in the bottom corners represent 5 μm, 2 μm and 2 μm for each magnification respectively. The cells at this stage are not confluent.

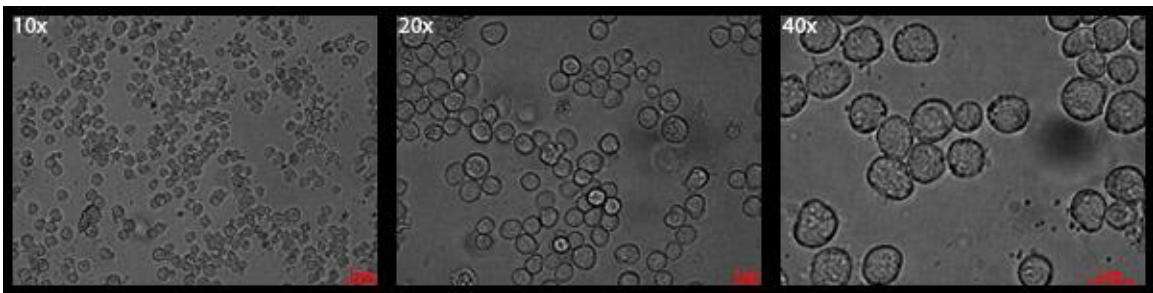


Figure 15: Sf21 monolayer culture after 2 days of growth under different magnifications (10×, 20× and 40× respectively). The red lines in the bottom corners represent 5 μm, 2 μm and 2 μm for each magnification respectively. The cells at this stage are becoming more confluent, however they are not ready to be sub-cultured just yet.

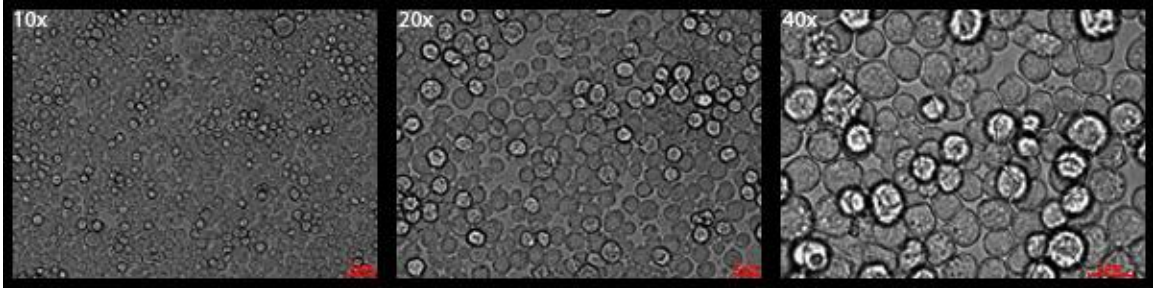


Figure 16: Sf21 monolayer culture prior to being sub-cultured (Day 4) under different magnifications (10 $\times$ , 20 $\times$  and 40 $\times$  respectively). The red lines in the bottom corners represent 5  $\mu\text{m}$ , 2  $\mu\text{m}$  and 2  $\mu\text{m}$  for each magnification respectively. The cells at this stage have become confluent and are ready to be sub-cultured.

Due to the figures being in black and white, it is hard to visualize the viability of the cells in the previous cell culture. However, Figures 14-16 do display the growth of cells and Figure 16 displayed the cells being around 90% confluent. Taking Figure 16 into consideration, the Sf21 suspension culture on day 4 could be used as a comparison (Figure 17).

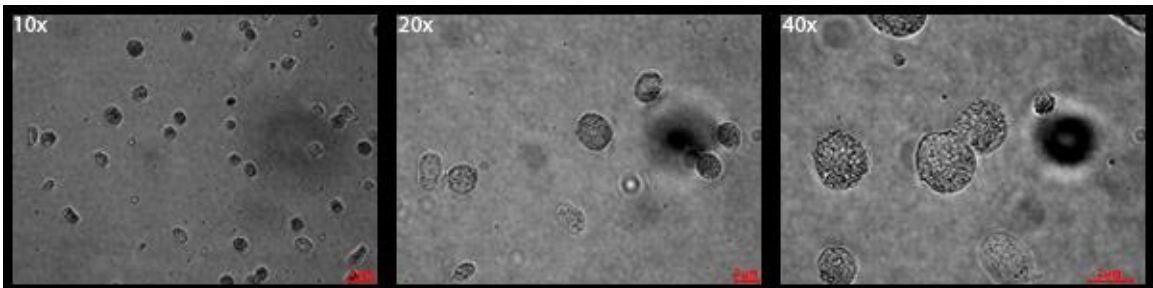


Figure 17: Sf21 suspension culture under different magnifications (10 $\times$ , 20 $\times$  and 40 $\times$  respectively) prior to being sub-cultured (Day 4). The red lines in the bottom corners represent 5  $\mu\text{m}$ , 2  $\mu\text{m}$  and 2  $\mu\text{m}$  for each magnification respectively. The cells have not ruptured and are circular in shape.

It is important to note that the shape of the Sf21 cells remained circular. Unhealthy/dead cells would show abnormal shapes including ruptured spheres similar to that of bloated infected cells (see section 3.2).

The current protocol for the growth of Sf21 suspension cell cultures incorporated the use of the New Brunswick Scientific Co. Incubator Shaker Series 25, a shaker incubator in E-Block (E-303). Prior to the use of this shaker incubator, the cell cultures were grown in New Brunswick Scientific Co. Incubator Shaker Series I26, a shaker incubator in the Cairns laboratory. However, unexpected and unknown contamination of small sphere like cultures occurred frequently.

While troubleshooting the contamination, the possibility of poor handling or lack of appropriate sterile technique was first suspected. After new stringent handling rules were set, the unknown contamination occurred again. The machines (shaker incubator and biological safety cabinet) and equipment handled were then suspected and were thoroughly surface disinfected using 100% bleach and a stronger disinfectant, Vikron. Despite this, the contamination occurred again at random stages of cell growth. Different surfaces of the laboratory environment were tested for contamination using a cotton swab test, in which cotton swabs were rubbed on different suspected surfaces (gloves, lab coats, biosafety cabinet, shaker incubator, etc.) and placed in 15 mL Falcon tubes holding 5 mL of culture medium. The cotton swab cultures were placed inside the bench top incubator set at 28°C. The cotton swab cultures showed negative results (i.e. no growth) except for the control, which was the cotton swab that was wiped with the contaminated suspension culture. Commercially supplied culture medium was also suspected and each time a culture showed evidence of contamination the culture medium was discarded and a new bottle was prepared.

Prior to the use of the new medium, the culture medium, FBS, pen-strep and fungizone were passed through a 0.45 micron filter in a sterile environment. However, this did not stop the occurrence of contaminated cultures. Antibiotics and fungizone concentrations were tripled to combat the contamination, but with no success.

Culture contamination became a great challenge for this research project as the contamination remained a mystery in both its frequency and identity. The greatest challenge was in the early identification of this contamination as it always occurred unexpectedly. Promisingly, early detection of contamination was possible by frequent physical examination of the cultures. During the handling of contaminated suspension cultures, a sweet smell was present. In addition, contaminated suspension cultures appear to be bright in color showing a white-yellow rather than the light yellow almost transparent color in healthy cells. Furthermore, a ring of cells at the air-water interface was observed in the suspension cultures. The further along the contamination was, the more distinct the layer became. Whenever a contamination was suspected, the culture was discarded according to the appropriate safety guidelines and a new culture was set up.

During one of the last few occurrences of contamination, the contaminated cell culture was plated on LB agar plates by Dr. Alan Castle and observed. His observation indicated the presence of a cocktail that included *Aspergillus sp.* and bacteria. At this stage and with the help of a colleague at Brock University, Dr. Mark Lukewich, new cultures were set up using different biosafety cabinet and grown in different incubators (New Brunswick Scientific Co. Incubator Shaker Series 25). With this change in environment, the frequency of contamination decreased drastically.

Monolayer cell cultures showed consistent healthy pattern of growth for 20-30 generations. When the growth pattern slowed, cell cultures were left to grow for another day, or a higher volume of cells was seeded or they were discarded and a new frozen stock culture was used. Suspension cultured cells that were not used for infection were seeded for the next suspension sub-culture. Healthy suspension cultures were able to be sub-cultured for 5-10 generations. Similarly, if suspension cultures showed a slower growth pattern, they were left to grow for another day, or a larger volume of cells was seeded, or the culture was discarded and a new suspension culture begun from a monolayer culture.

### **3.2. Baculovirus Infection of Sf21 Cells (Expression of OSBP and Baculovirus)**

When healthy suspension cultures were obtained,  $4.5 \times 10^8$  cells were isolated and set for infection. Initial stocks of baculovirus were provided by Dr. Neale Ridgway (Dalhousie University, Halifax) with pre-calculated titre values. A titre of 0.15 was found to be optimal for OSBP expression in combination with an infection incubation period of 72 hours. Successful trials of infections yielded protein and a subsequent generation of baculovirus. Baculovirus was located in the supernatant of the cell pellet that was made upon the completion of the infection. The collected supernatant was passed through a 0.22 micron filter and a plaque assay was performed in order to calculate its viral yields. Unfortunately, in several failed plaque assays attempts, the titre values of collected baculovirus could not be determined. Subsequent infections incorporated an estimated volume of baculovirus (0.5 mL – 2 mL) to be added and after multiple successful trials based of protein expression, the optimal value was determined to be 1 mL. Upon the completion of the infection stage, the cells were observed under a microscope and were typically larger in size (Figures 18-19).

For the best expression of OSBP, the Sf21 infected cells had increased significantly in size in shape yet were not ruptured.

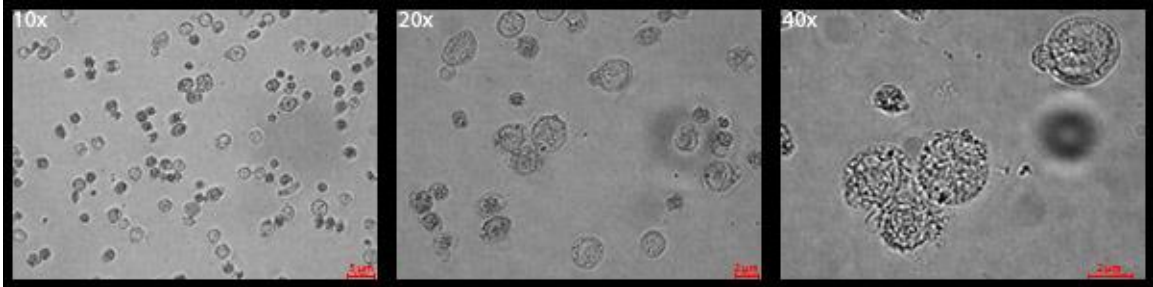


Figure 18: Day 3 (72 hours) of Sf21 suspension culture infected with OSBP-S5E baculovirus provided by Dr. Neale Ridgway under different magnifications (10x, 20x and 40x respectively). The red lines in the bottom corners represent 5  $\mu\text{m}$ , 2  $\mu\text{m}$  and 2  $\mu\text{m}$  for each magnification respectively. Upon a complete infection, the cells have increased in size to 1.5 – 2 times bigger in diameter.

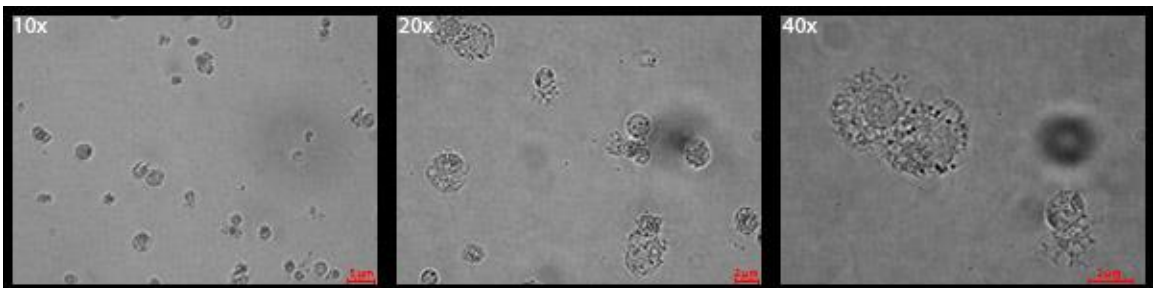


Figure 19: Day 3 (72 hours) of Sf21 suspension culture infected with OSBP-S5E baculovirus obtained from the filtered supernatant of a pre-infected culture under different magnifications (10x, 20x and 40x respectively). The red lines in the bottom corners represent 5  $\mu\text{m}$ , 2  $\mu\text{m}$  and 2  $\mu\text{m}$  for each magnification respectively. Upon a complete infection, the cells have increased in size to 1.5 – 2 times bigger in diameter. Few of the cells have ruptured and lost their circular shape.

The best method to define the success of the infection (i.e. expression of OSBP) was to examine the infected cells under a microscope prior to pelleting. Too many ruptured cells would indicate that the infected cells were left for too long or too much baculovirus was added. Too little or no bloated cells would indicate very little to no infection and thus poor expression of OSBP. This indicated that too little baculovirus was used, or the baculovirus stock was too old (usually after 8 months of storage) and became inefficient. Alternatively, the infection period was too short and a 96-hour incubation period should be considered. Cultures of potentially successful expression of OSBP were pelleted and stored at  $-80^{\circ}\text{C}$ .

### **3.3. Purification of OSBP**

While a successful expression of OSBP could be judged through an observation of the cells prior to their centrifugation (see section 3.2), this method was at times inaccurate. Occasionally, what appeared to be successfully infected cells resulted in a very low or no yield of protein. The success of an OSBP expression could only be determined after the purification process was done.

The initial protocol for the purification process started with mixing one OSBP pellet (~5 mL volume, ~2 g mass of wet cells) representing cells collected from 250 mL of infected cell culture with 5 mL of metal-affinity resin. However, the expression of OSBP-S5E protein was relatively low (about half the amount) in comparison to wt-OSBP (estimates of protein yield can be found in section 3.4 – table 2). Given the low expression of desired protein, other proteins were often found non-specifically bound to the resin during the purification process (Figure 22). This could be mostly avoided by combining two pellets for 5 mL of resin, which yielded higher purity of the recovered protein.

During the purification process, the FPLC program (Bio-Rad BioLogic DuoFlow) measured the absorbance values of the eluted sample in real time. Looking at Figures 20 and 21, which highlight regions in which the washes and elution of protein were observed at 280 nm. The absorbance at 280 nm starts at a high value (~2.5) when the unbound protein fraction was passing through the column as the first wash was applied (0-20 min). The second region (20-30 min) was when the low imidazole buffer wash was passing through the column, while the third region (30-40 min) was when the high imidazole elution buffer was passing through the column. The presence of protein can be observed through a small yet significant increase (hump like shape) as seen in a good case of expression (Figure 21).

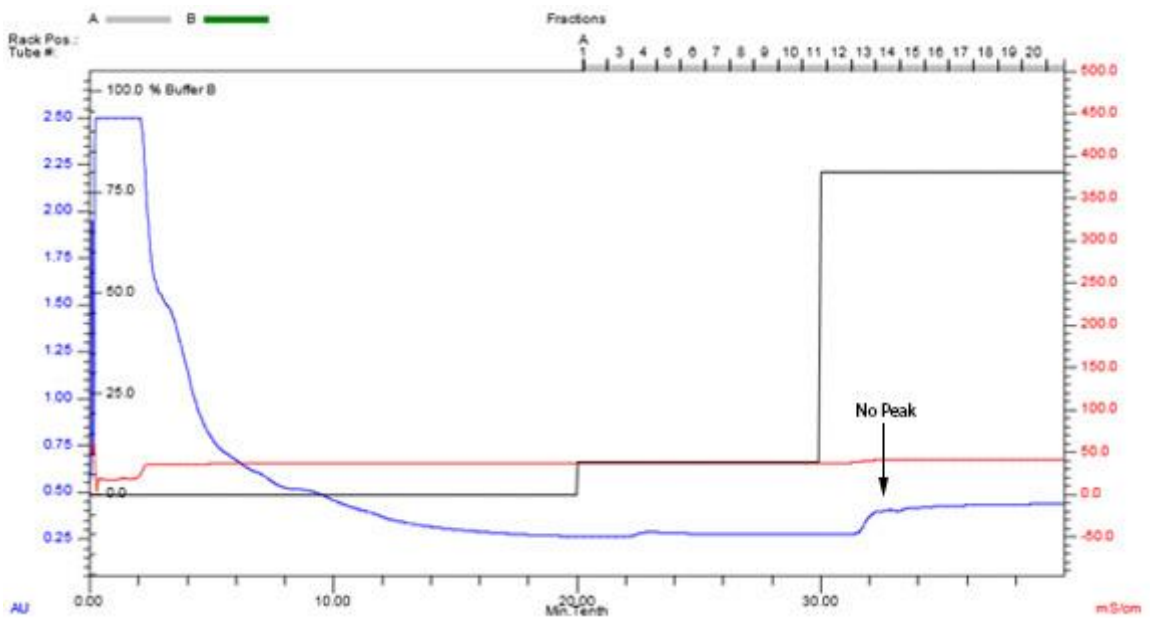


Figure 20: Absorbance at 280 nm, conductivity (mS/cm) and change in buffer B of the sample that passed through IMAC column during very low expression of S5E (1 pellet of OSBP-S5E with 5 mL of resin). The distinct protein peak was absent.

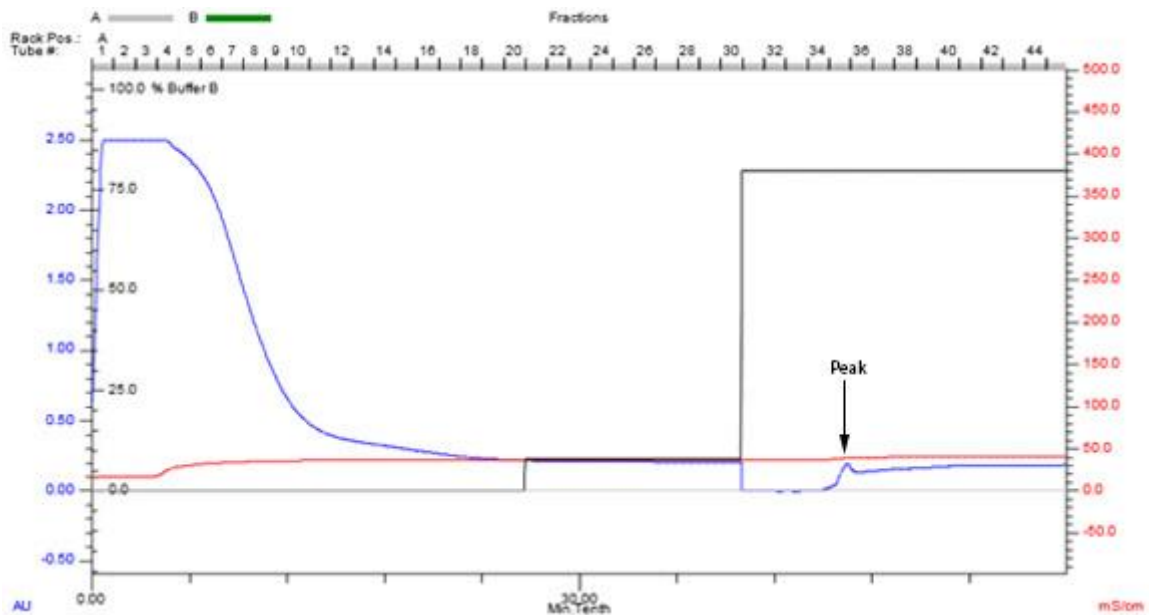


Figure 21: Absorbance at 280 nm, conductivity (mS/cm) and change in buffer B of the sample that passed through IMAC column during a good expression of S5E (2 pellet of OSBP-S5E with 5 mL of resin). The distinct protein peak was present.

A similar purification to that of Figure 21 was analyzed under SDS-PAGE with the resulting gel picture of Figure 22. The presence of the peak in fractions 35-36 with the corresponding analysis under SDS-PAGE confirms the presence of OSBP-S5E. The size of the OSBP-S5E protein bands was approximately ~90 kDa which is similar to that reported by Goto, *et al.* (27).



Figure 22: SDS-PAGE of OSBP-S5E purification by cobalt affinity column through an automated process using the FPLC machine Bio-Rad BioLogic DuoFlow; where PM is the protein marker (New England BioLabs), CL is the cell lysate, FT is the flow-through, F# is the fraction number, wash 1 is the first wash with no imidazole, wash 2 is the second wash with 20 mM imidazole, and eluted fractions is the purified protein eluted using 200 mM imidazole. OSBP-S5E was prominent in fractions 35 and 36.

### 3.4. OSBP Quantification

Purified fractions of OSBP were quantified by Bradford assay. Bradford reagent (Sigma-Aldrich), and 50  $\mu$ L of a purified sample were mixed and the absorbance measured at 595 nm. The concentration of the protein was calculated based on the regression analysis of the linear portion of the curve. Known concentrations of bovine serum albumin (BSA) were used and a calibration curve was constructed yielding an equation of  $y=1.0275x$ , in

which y is the absorbance at 595 nm and x is concentration of protein sample in mg/mL (Figure 23).

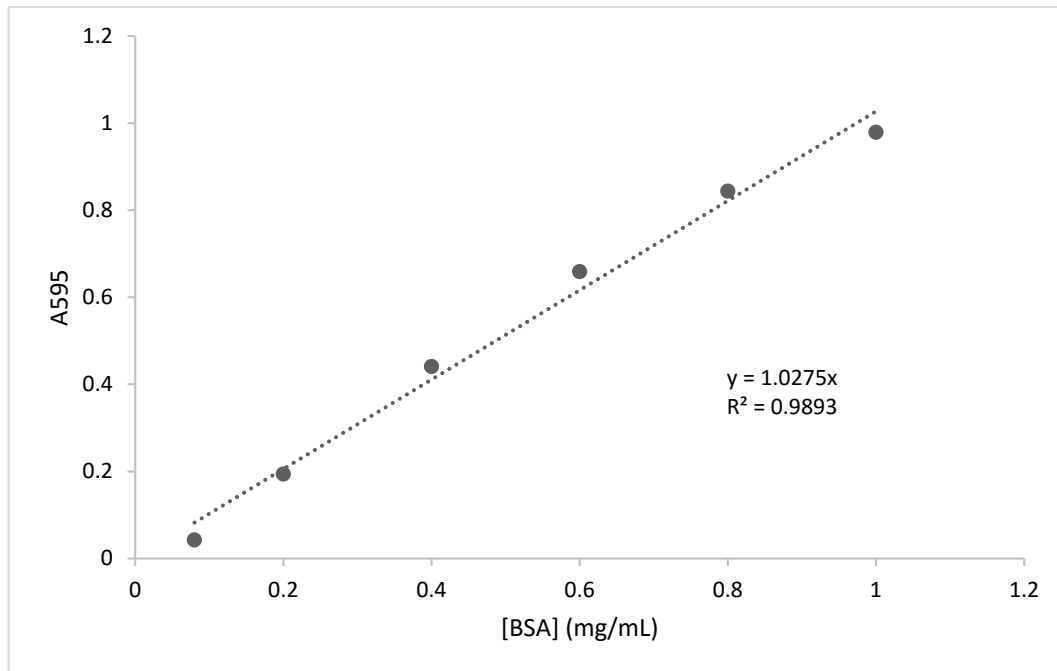


Figure 23: Bradford assay calibration curve constructed using known concentrations of BSA and absorbance at 595 nm (courtesy of Parthajit Mukherjee).

The amount of purified OSBP-S5E for a few of the attempts made are reported in Table 2. These values were measured after the buffer exchange was done (from imidazole elution buffer to DPI buffer) and the protein was concentrated using Amicon Ultra Centrifugal Filters Ultracel – 50K. On average, approximately 0.4 mg of protein was eluted per purification process of 2 pellets at a time.

Table 2: Recovery of OSBP-S5E. The amount of purified OSBP-S5E per 2 pellets per purification and their corresponding dates determined using the Bradford assay. Reported are absorbance at 595 nm (A595), the concentration of OSBP-S5E in mg/mL and  $\mu$ M, the volume of purified fractions in mL and the mass of purified OSBP-S5E in mg.

Attempt	Corresponding Date	A595	[OSBP-S5E] (mg/mL)	[OSBP-S5E] ( $\mu$ M)	Volume of Fraction (mL)	Mass of OSBP-S5E (mg)
1	Mar 19/2015	0.176	0.171	1.90	3.87	0.663
2	Mar 19/2015	0.069	0.067	0.75	3.87	0.260
3	Jul 28/2015	0.198	0.193	2.14	2.10	0.405
4	Nov 3/2015	0.128	0.125	1.38	1.18	0.145
Average		0.143	0.139	1.54	2.76	0.369

### 3.5. Ion-Exchange Chromatography

During the first attempted purification of OSBP-S5E, multiple contaminating bands (~30-45, 60 kDa) with less intensity than the 90 kDa OSBP protein were observed in the purified fractions. With the hope of further purifying OSBP-S5E, ion exchange chromatography was attempted. Using DEAE Sepharose resin (Bio-Rad Macro-Prep DEAE Support Weak Anion Exchange Support), the column was prepared as described in section 2.4.9. The resin (3 mL) was centrifuged at 4000 x g using a Beckman Coulter Allegra X-30R Centrifuge SX4400 rotor for 5 minutes and the storage buffer was discarded. The resin

was then washed twice with distilled water, followed by another two washes using the running buffer (RB – 50 mM Tris, pH 8.5) and equilibrated with the running buffer overnight. The resin was then transferred to a Bio-Rad glass column (similar to that used in purification of protein) and the resin was left to settle by gravity. The purified S5E protein fractions were then loaded onto the column and the column apparatus was setup and transferred to the FPLC machine (Bio-Rad BioLogic DuoFlow) for an automated protocol. OSBP-S5E was exposed to the combination of a running buffer (RB) and a salt buffer (SB) in order to create three different concentrations of salt (20 mM, 250 mM and 500 mM NaCl). 50 mL of a low salt wash (90% running buffer (RB), 10% salt buffer (SB)) was passed through the column first in order to wash any non-specific binders. The concentration of salt was then increased to 250 mM and 20 mL of a medium salt wash (50% RB, 50% SB) was then passed through the column as to elute the OSBP-S5E protein. The concentration of salt was increased again to 500 mM NaCl and 30 mL of a high salt wash (100% SB) was passed through the column as to ensure no protein was still bound to the column.

The flow rate was set to 1 mL/min and all eluted samples were collected and analyzed for purity. The purification process was automated through the FPLC machine in which the sample passing through the column was monitored by the change in absorbance at 280 nm and the change in conductivity.

Variability in the monitored absorbance and conductivity during the purification process was observed in which multiple sudden changes in absorbance and conductivity occurred. This was due to the input versus output flow rate of the column. Although the FPLC machine was set to flow at rate of 1 mL/min, it was only the sample input (into the column) flow rate that was consistent with the FPLC machine setting. The output (leaving

the column) flow rate could not be controlled by the FPLC machine and was drastically affected by the resin and the packing of the column. Although the resin was packed by just using gravity, the resin did slow the output flow rate resulting in a backlog of wash buffer, which collected on top of the resin. The resulting backlog of wash buffer changed the concentration of the salt that was passing through the resin. In other words, without the backlog of the buffer, each drop of wash buffer entering the column would almost directly touch the resin and, for example, at the start of the medium salt wash, the change in salt concentration changes immediately from 20 mM to 250 mM. However, when the backlogged buffer is present, the salt concentration does not directly change from 20 mM to 250 mM; but rather changes from 20 mM to 250 mM gradually. This results in the OSBP-S5E being eluted in a diluted fashion and over multiple fractions. At times like this, the input flow rate was decreased to 0.1 mL/min to allow the backlogged buffer to pass through the resin. It was necessary at times to pause the protocol (i.e. input flow rate of 0 mL/min) or take apart the column in order to allow the backlogged buffer to pass through. This was a challenge as the output flow rate did decrease after a short period of time from changing the input flow rate. After multiple adjustments, the best flow rate that gave the most stable input/output flow rate was 0.35 mL/min.

SDS-PAGE was performed on samples from the collected fractions of the ion exchange chromatography (Figure 24). The SDS-PAGE gel (Figure 24) showed that there was little to no change in the purity of the protein samples that had passed through the ion exchange chromatography.

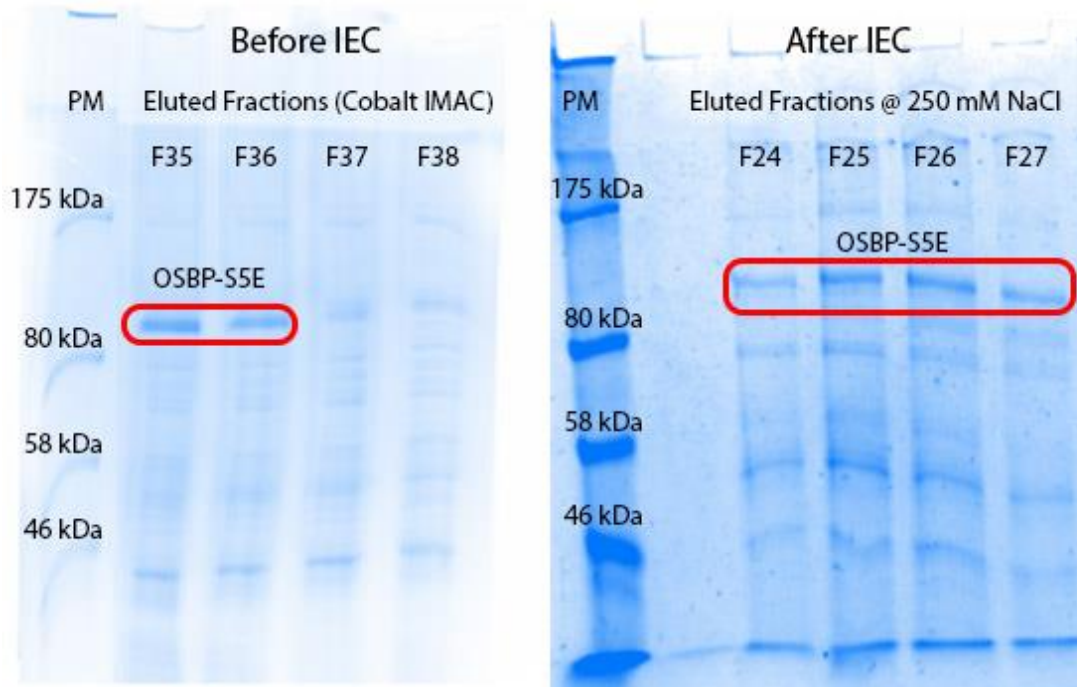


Figure 24: SDS-PAGE of OSBP-S5E purification by ion exchange chromatography (using Bio-Rad Macro-Prep DEAE Support Weak Anion Exchange Support) through an automated process using the FPLC machine (Bio-Rad BioLogic DuoFlow). This purification was done after the OSBP-S5E was purified by a cobalt affinity column. The ‘Before IEC’ gel was adapted from Figure 22. PM is the protein marker (New England BioLabs), F# is the fraction number, and eluted fractions are the purified protein. OSBP-S5E was prominent in fractions 35 and 36 before IEC and fractions 24 to 27 after IEC. Please note that the samples used for the IEC were not the same samples as the ‘Before IEC’ samples. However all samples were of OSBP-S5E but of two different purifications.

Due to the multiple challenges that arose during the first attempt of OSBP-S5E ion exchange chromatography, another attempt was made to a newly purified protein. However, the ion exchange chromatography showed no improvement in the purity of OSBP-S5E

protein. This was in accordance with an attempt previously made by Parthajit Mukherjee with wt-OSBP in which the result was the same.

### **3.6. DPI – Membrane Lipid-Protein Binding Assay**

The behavior of the binding kinetics of OSBP to different compositions of lipid bilayers was examined by dual polarization interferometry. Lipid vesicles (~100 nm in size, 0.5 mM) extruded using 100 nm polycarbonate membrane filters were injected into the DPI machine using a programmable pump and across the sensor chip. During contact with the chip the vesicles adsorbed and flattened forming a single bilayer on top of the silicon oxynitride chip (42). The adsorption of 1.0  $\mu\text{M}$  of OSBP to lipids of varying composition was analyzed at a flow rate of 25  $\mu\text{l}/\text{min}$  over the period of ~600 s. Controls were previously done by Parthajit Mukherjee and other colleagues to determine which concentrations of lipids and protein to use at this flow rate and observation time window.

The work that was done with  $\alpha$ -tocopherol transfer protein ( $\alpha$ -TTP) in our laboratory using dual polarization interferometry set the ground rules in the interpretation of the DPI results (43; 44; 45). Baptist *et al.* have demonstrated that  $\alpha$ -TTP, which binds well to bilayers, formed an adsorbed protein mass of ~0.75  $\text{ng}/\text{mm}^2$  when 1.0  $\mu\text{M}$  of  $\alpha$ -TTP was exposed to an immobilized bilayer of 9:1 DOPC:DOPS (45). Values of adsorbed protein mass lower than that can be viewed as a relatively poor membrane binding protein.

The binding of OSBP to DOPC lipid membranes showed only a small change in specific binding mass (represented by protein binding to the immobilized bilayer) for both wt-OSBP and OSBP-S5E (Figure 25). The binding of both wt-OSBP and OSBP-S5E to an immobilized DOPC bilayer formed an adsorbed protein mass of ~0.5  $\text{ng}/\text{mm}^2$  (Figure 26);

making OSBP, regardless of its phosphorylation state, a somewhat poor binder to neutral PC bilayers.

Upon injection of the protein sample, the adsorbed protein mass rapidly increases reflecting a temporary formation of layer that quickly dissociates once the injection has ended (indicated by arrow) (Figure 25). This does not necessarily represent the binding of protein to the immobilized lipid bilayer, but rather could be the protein floating on top or near the lipid bilayer that caused the change in signal. This behavior in combination with a low ( $\leq \sim 0.5 \text{ ng/mm}^2$ ) adsorbed protein mass value can be interpreted as a relatively poor binding protein to that lipid composition; such was the case in wt-OSBP and OSBP-S5E on DOPC bilayers (Figure 26). In addition, layers lower than  $\sim 0.3 \text{ ng/mm}^2$  are considered unreliable and were not taken in consideration.

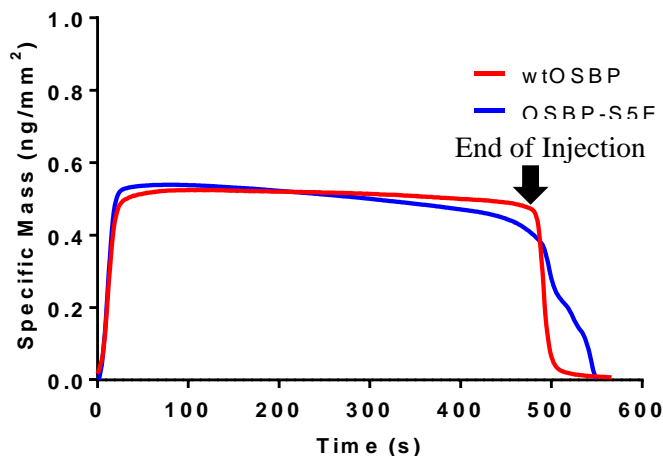


Figure 25: Real time association of  $1.0 \mu\text{M}$  of wt-OSBP and OSBP-S5E with DOPC neutral bilayer. The adsorbed protein mass quickly increased at the beginning of the injection of protein and quickly decreased at the end of the injection. The behavior of wt-OSBP with DOPC bilayer was similar to that of OSBP-S5E.

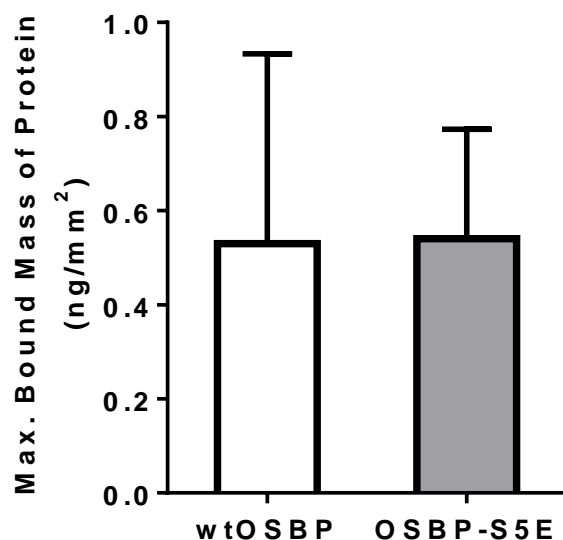


Figure 26: Maximum adsorbed mass of 1.0  $\mu\text{M}$  wt-OSBP and OSBP-S5E to an immobilized neutral DOPC bilayer (courtesy of Parthajit Mukherjee). Regardless of phosphorylation state, OSBP adsorbed to an approximate 0.5  $\text{ng}/\text{mm}^2$  adsorbed mass of protein. Both samples were run in duplicates.

The binding of wt-OSBP and OSBP-S5E to PI(4)P containing lipid membranes are different (Figure 27-28). The behavior of wt-OSBP on 2% PI(4)P containing lipid membranes showed a gradual increase in adsorbed mass, followed by a slower gradual decrease over time before the end of injection (Figure 27). For OSBP-S5E, such behavior was absent and instead a rapid increase at the start of the flow of protein and a rapid decrease at the end of the flow of protein were observed (Figure 28). Wt-OSBP adsorbed with high affinity to PI(4)P containing bilayers and the adsorbed mass of wt-OSBP increased with increasing percentages of PI(4)P (Figure 27). The slow desorption of wt-OSBP from PI(4)P containing membrane may indicate that wt-OSBP was first adsorbing then extracting PI(4)P from the lipid bilayer. As the bilayer is depleted of PI(4)P lipids, the affinity of wt-OSBP

for the bilayer membrane then returns to that for a DOPC bilayer (Figure 25). The absence of such behavior (the quick increase followed by gradual decrease in adsorbed protein mass) in OSBP-S5E (Figure 28) may indicate that the phosphorylation of those 5 serine residues (S5E) prevents lipid recognition and/or PI(4)P extraction. Additional tests, such as mass spectrometry, which could identify PI(4)P through its mass peak, on collected fractions and/or antibody detection methods for PI(4)P, are needed to confirm the extraction process.

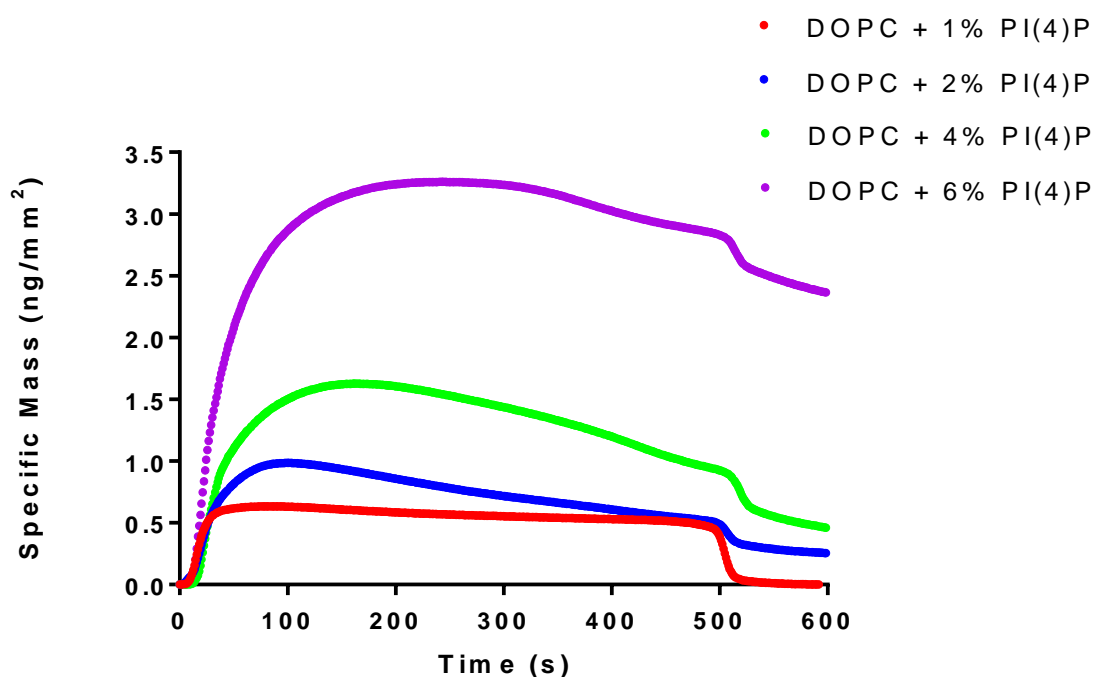


Figure 27: Real time association of 1.0 μM of wt-OSBP with a DOPC bilayer containing varying concentrations of PI(4)P (1-6%). Wt-OSBP adsorbed with high affinity to PI(4)P containing bilayers and the adsorbed mass of wt-OSBP increased with increasing percentages of PI(4)P. This was followed by a slow desorption of wt-OSBP from PI(4)P containing membranes.

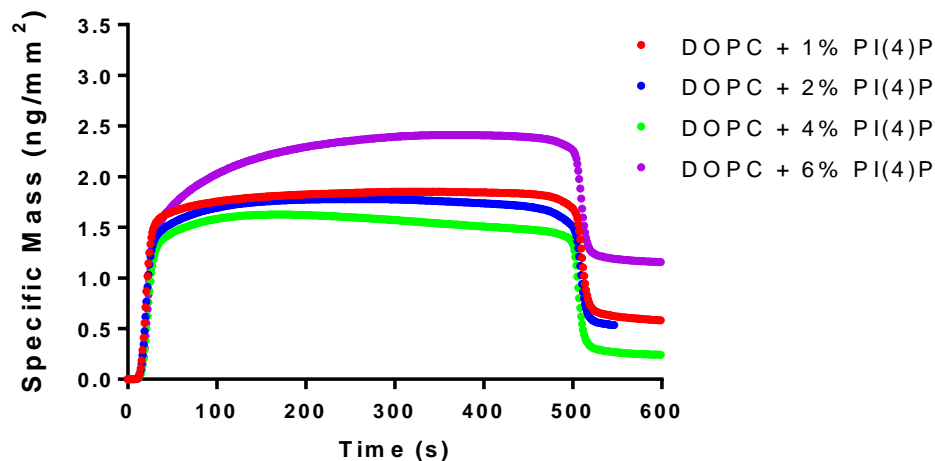


Figure 28: Real time association of 1.0  $\mu\text{M}$  of OSBP-S5E with DOPC bilayer of varying concentrations of PI(4)P (1-6%). OSBP-S5E adsorbed quickly to PI(4)P containing bilayers upon injection of protein and quickly desorbed from PI(4)P containing membranes upon the completion of the injection. Increased PI(4)P percentages did not significantly change specific bound mass of OSBP-S5E to PI(4)P containing bilayers except slightly in the case of 6% PI(4)P likely due to protein sticking longer due to excess PI(4)P.

In the presence of sterol, the overall binding behavior of OSBP, regardless of phosphorylation state, was fairly similar (Figures 29-32). Though the maximum specific binding mass of OSBP to cholesterol- versus oxysterol-containing membranes differed, it did not differ in terms of varying the concentration of the sterol that was present (Figure 33). In other words, regardless of the concentration of sterol that was present, the maximum specific binding mass was the same. On the other hand, comparing the behavior of OSBP with cholesterol containing membranes and oxysterol containing membranes, it was interesting to note that both wt-OSBP and OSBP-S5E showed nearly 2-fold higher maximum specific bound mass for cholesterol than that of the oxysterol (25-

hydroxycholesterol). Interestingly, this was unexpected as literature from Dawson *et al.* showed 25-hydroxycholesterol to have a higher affinity to ORPs than cholesterol does (46; 47). Although OSBP does adapt its affinity differently to cholesterol than to 25-hydroxycholesterol, it is still unclear as to why or how that happens.

With the absence of the wt-OSBP-PI(4)P binding behavior, it can be speculated that the sterols were not extracted regardless of phosphorylation state. In the case of wt-OSBP and PI(4)P containing lipid bilayers, there was a quick and high adsorption of wt-OSBP to PI(4)P membranes followed by a slow desorption. In the cases of all other tests, desorption of OSBP (rapid desorption) happens only at the end of the injection sample flow, and the absence of such desorption behavior (slow desorption) likely indicates the absence of an extraction of a ligand. This was the behavior of OSBP (regardless of its phosphorylation state) in the presence of varying concentrations of cholesterol and oxysterol. The association of OSBP with helper proteins such as VAP-A likely indicates that OSBP, regardless of its phosphorylation state, cannot extract sterols without the presence of helper proteins such as VAP-A (48).

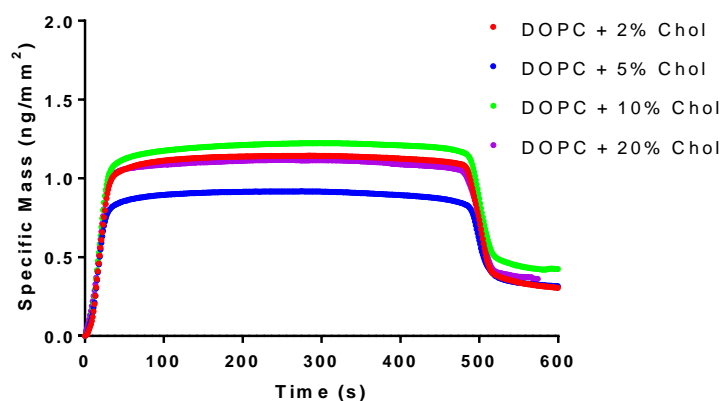


Figure 29: Real time association of 1.0  $\mu\text{M}$  of wt-OSBP with DOPC bilayer of varying concentrations of cholesterol (2-20%). Wt-OSBP adsorbed quickly to cholesterol containing bilayers upon injection of protein and quickly desorbed from cholesterol containing membranes upon the completion of the injection. Increased cholesterol percentages did not change specific bound mass of wt-OSBP to cholesterol containing bilayers.

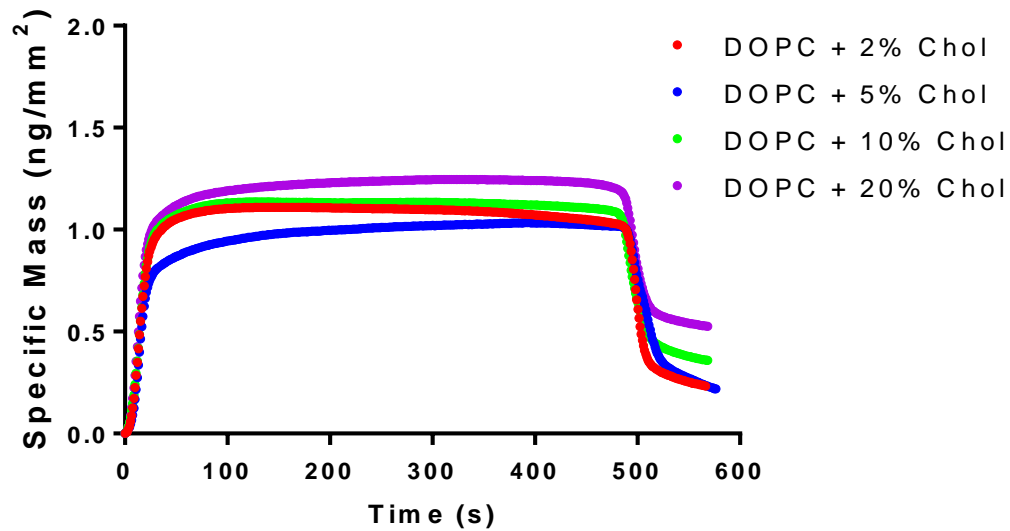


Figure 30: Real time association of 1.0  $\mu\text{M}$  of OSBP-S5E with DOPC bilayer of varying concentrations of cholesterol (2-20%). OSBP-S5E adsorbed quickly to cholesterol containing bilayers upon injection of protein and quickly desorbed from cholesterol containing membranes upon the completion of the injection. Increased cholesterol percentages did not change specific bound mass of OSBP-S5E to cholesterol containing bilayers.

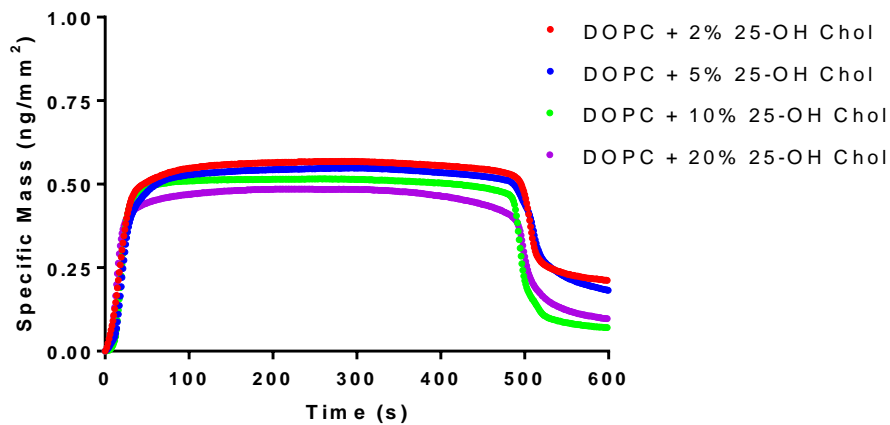


Figure 31: Real time association of 1.0  $\mu\text{M}$  of wt-OSBP with DOPC bilayer of varying concentrations of 25-hydroxycholesterol (2-20%). Wt-OSBP adsorbed quickly to 25-hydroxycholesterol containing bilayers upon injection of protein and quickly desorbed from 25-hydroxycholesterol containing membranes upon the completion of the injection. Increased 25-hydroxycholesterol percentages did not change specific bound mass of wt-OSBP to 25-hydroxycholesterol containing bilayers.

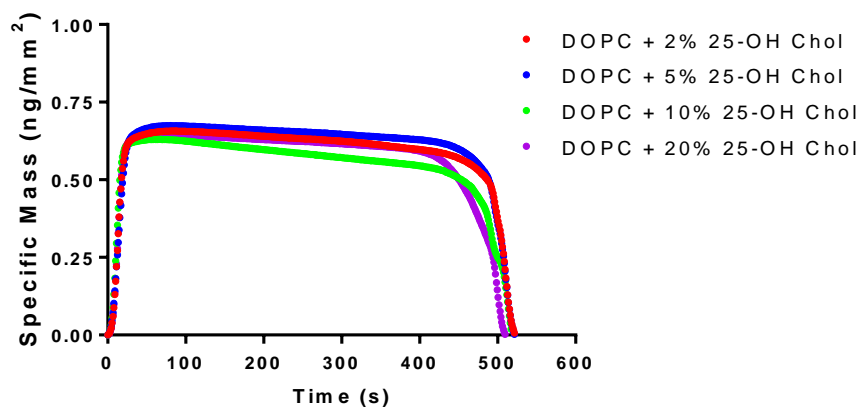


Figure 32: Real time association of 1.0  $\mu\text{M}$  of OSBP-S5E with DOPC bilayers of varying concentrations of oxysterol (2-20%). OSBP-S5E adsorbed quickly to 25-hydroxycholesterol containing bilayers upon injection of protein and quickly desorbed from 25-

hydroxycholesterol containing membranes upon the completion of the injection. Increased 25-hydroxycholesterol percentages did not change specific bound mass of OSBP-S5E to 25-hydroxycholesterol containing bilayers. In comparison to wt-OSBP, these results are similar thus indicating that the behavior of OSBP-S5E is similar to wt-OSBP in the presence of 25-hydroxycholesterol membranes.

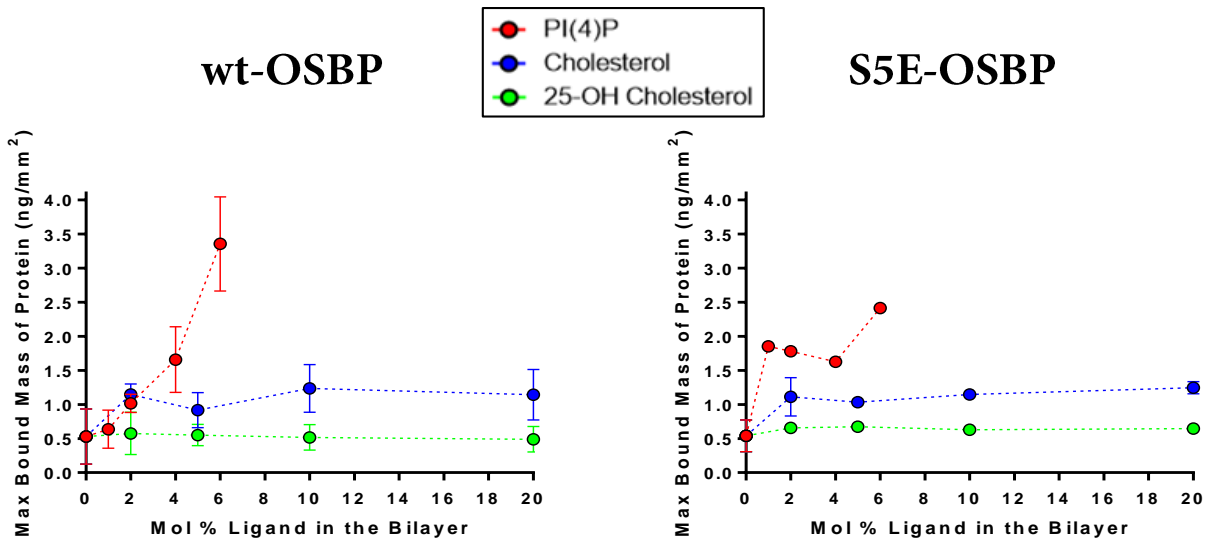


Figure 33: Maximum bound mass of 1.0  $\mu$ M OSBP with increasing molecular percentage of ligand (PI(4)P, cholesterol and 25-hydroxycholesterol) in the adsorbed layer (courtesy of Parthajit Mukherjee). The maximum adsorbed mass of wt-OSBP increased as the concentration of PI(4)P in the lipid bilayer increased. The maximum adsorbed mass of OSBP, regardless of phosphorylation state, did not significantly differ as the concentration of sterol increased. However, OSBP, regardless of phosphorylation state, showed almost 2-fold a greater adsorbed mass when bound to cholesterol in comparison to 25-hydroxycholesterol.

## 3.7. Fluorescent Based Assays

### 3.7.1. Binding Assay

Fluorescence binding assays that monitored the association of 22-NBD-cholesterol to 0.2  $\mu$ M of OSBP were also attempted. Quadruplicates of wt-OSBP were monitored along with OSBP-S5E and a blank (i.e. no protein) sample (Figure 34). Upon examination, wt-OSBP showed an increase in fluorescence intensity to a maximum of around 4500 counts with  $\sim$  125 nM of 22-NBD cholesterol. The binding curve displayed by the wt-OSBP represented one-site binding. Due to the variability in the fluorescent intensity ( $\pm$   $\sim$ 1000 counts) for the wt-OSBP, the data was normalized and re-plotted; excluding OSBP-S5E as its intensity and trend was no different than that of the blank sample (Figure 35). OSBP-S5E showed a similar trend to the blank sample in which no change in fluorescence was observed suggesting that -22NBD-cholesterol did not bind to S5E-OSBP. Hence, we conclude that OSBP-S5E does not bind 22-NBD-cholesterol. The data obtained were fit to a one-site binding non-linear regression using Prism (GraphPad, Inc) according to the equation below.

$$Y = B_{\max} * X / (K_d + X)$$

One-site binding, non-linear regression model where Y is the fluorescent intensity,  $B_{\max}$  is maximal binding,  $K_d$  is dissociation constant (concentration of ligand at which half-maximal binding is reached), and X is the concentration of ligand. A dissociation constant,  $K_d$ , of  $15 \pm 1.4$  nM for 22-NBD-cholesterol binding to wt-OSBP was determined.

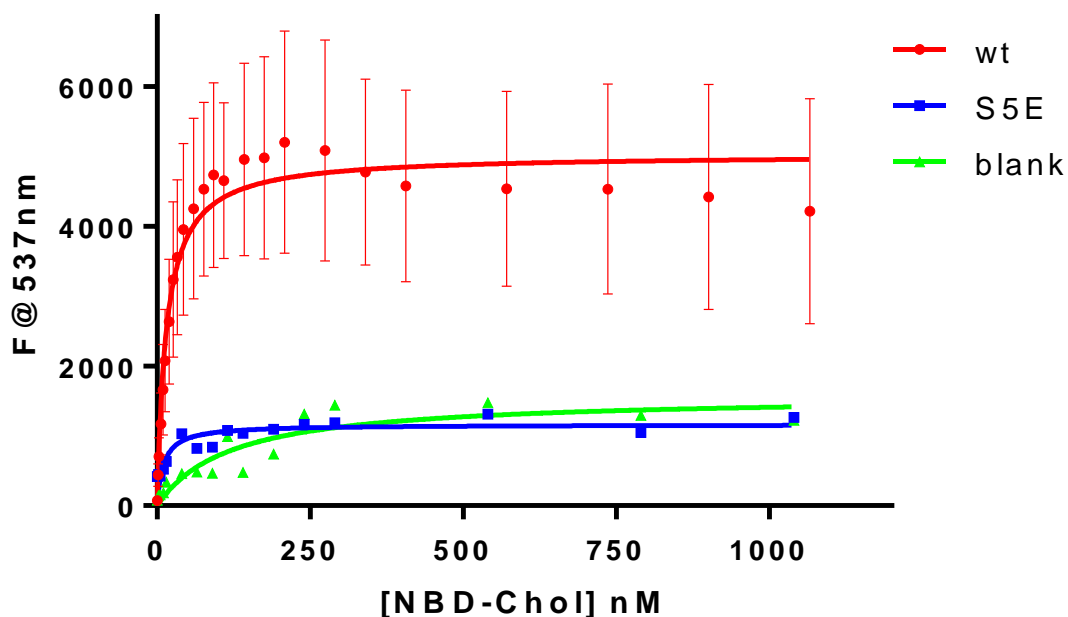


Figure 34: Binding assay of wt-OSBP and OSBP-S5E with 22-NBD-cholesterol using fluorescent at 537 nm and one site non-linear regression model (Prism, GraphPad). The quadruplicates of wt-OSBP showed significant variability in the recorded fluorescence, resulting in large error bars ( $\pm \sim 1000$  counts) of the fluorescent intensity. The binding behavior of OSBP-S5E was similar to the blank sample with fluorescent intensity of  $< 1500$  counts.

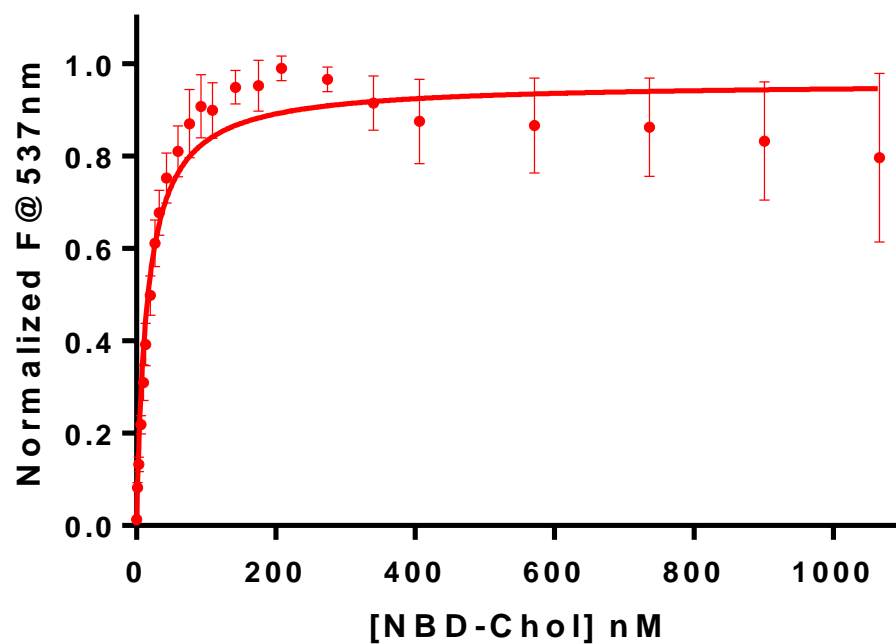


Figure 35: Normalized fluorescence data for the binding assay of wt-OSBP (in quadruplicate) with 22-NBD-cholesterol using fluorescence at 537 nm and one site non-linear regression model (Prism, GraphPad). The quadruplicates of wt-OSBP showed a similar behavior to that of a one site binding non-linear regression model but with smaller variability in the error bars ( $\pm \sim 0.1$ ) of the fluorescent intensity.

#### 4. CONCLUSION AND FUTURE DIRECTIONS

The proposed mechanism (15) of OSBP as a PIP-sterol transport/exchanger and the localization of OSBP at the Golgi through its phosphorylation state, prompted us to explore OSBP's binding behavior to different lipid compositions. Both wt-OSBP and the phosphomimic OSBP-S5E were looked at. Using dual polarization interferometry, DOPC lipid bilayers with different compositions of PI(4)P and sterols (cholesterol and 25-hydroxycholesterol) were immobilized and the binding behavior of OSBP was examined in real time. Using a fluorescence-based binding assay, OSBP's binding affinity to 22-NBD-cholesterol was also examined.

The results obtained from the DPI tests revealed that wt-OSBP quickly adsorbs to PI(4)P containing membranes followed by a gradual desorption. This distinct behavior likely indicates that wt-OSBP was extracting PI(4)P and subsequently leaving the lipid bilayer. This distinct behavior was absent in all other tests performed using the phosphomimic mutant OSBP-S5E either with PI4P or either of the sterols used. The absence of such binding behavior, i.e. the rapid increase and the formation of a peak followed by a gradual decrease binding behavior, in the case of OSBP-S5E and PI(4)P containing membrane suggested that the phosphorylation of OSBP may prevent the recognition and/or extraction of PI(4)P.

In the presence of sterols, the overall binding behavior of OSBP, regardless of phosphorylation state, was fairly similar. The maximum specific bound mass of OSBP to sterol containing bilayers did not change as the concentration of sterols increased. However, comparing the maximum specific bound mass of OSBP to cholesterol containing bilayers

with oxysterol (25-hydroxycholesterol) containing bilayers, OSBP displayed nearly a 2-fold increase in bound mass.

In addition, the ligand recognition ability of OSBP was further tested using a fluorescence-based binding assay. Using 22-(*N*-(7-nitrobenz-2-oxa-1,3-diazol-4-yl)amino)-23,24-bisnor-5-cholesterol-3 $\beta$ -ol (22-NBD cholesterol), wt-OSBP displayed a one site binding behaviour with a dissociation constant  $K_d$ , of  $15 \pm 1.4$  nM. OSBP-S5E did not bind well to 22-NBD cholesterol and the fluorescence intensity was similar to that of a blank sample (<1500 counts).

For future directions, it is suggested to first perform additional tests to confirm the extraction of PI(4)P by wt-OSBP using either mass spectrometry or anti-PI(4)P antibodies. Effluent leaving the DPI machine can be collected and assessed or, better yet, after a test of wt-OSBP on PI(4)P containing membrane using the DPI, the chip holding the immobilized lipid bilayer can be taken out of the machine and then the remaining lipid bilayer removed. The recovered lipids can then be tested for the presence (or lack) of PI(4)P which should be the case if wt-OSBP was extracting PI(4)P lipids.

In addition, further replicates of the protein-lipid binding assays using OSBP-S5E are needed. The results of OSBP-S5E stated here were reported after one or two tests were made. A minimum of three replicates, such was the case of wt-OSBP, are needed to better and more accurately report the results.

It is also important to perform protein lipid binding assays using the DPI in which OSBP is pre-incubated with PI(4)P or sterol and see if the OSBP can exchange that ligand if exposed to sterol or PI(4)P containing membrane. Assuming that the OSBP does not

require any helper proteins (in the case of wt-OSBP and PI(4)P), the exchange of a sterol with PI(4)P should be observed in the case of a pre-incubated wt-OSBP with cholesterol being exposed to PI(4)P containing membrane. If this was the case, the binding behavior through real time, i.e. the DPI curve, should look similar to that of when a ligand is being extracted (e.g. the DPI curve of wt-OSBP and PI(4)P containing membranes).

Additional fluorescence based assays with 22-NBD cholesterol can be performed in which Förster resonance energy transfer (FRET) in a FRET transfer assay can be looked at. Pre-incubating OSBP with 22-NBD-cholesterol and mixing the complex with a vesicle population containing a fluorescence quencher can show if OSBP can transfer 22-NBD-cholesterol into lipid vesicles.

In conclusion, wt-OSBP and OSBP-S5E bound in a similar fashion to sterol-containing lipid bilayers. On the other hand, in the presence of PI(4)P-containing lipid bilayers, the wt-OSBP bound differently. We suspect that PI(4)P is extracted by wt-OSBP, however, this needs to be further examined and confirmed. Relating all of this to the bigger picture and the proposed pathway, we suspect that phosphorylation is the facilitator in the process of PI(4)P lipid extraction. However, it is still unclear what the role of phosphorylation of OSBP is in the presence of sterols.

## 5. REFERENCES

1. Ridgway, N. D., Lagace, T. A., Cook, H. W., & Byers, D. M. (1998). Differential effects of sphingomyelin hydrolysis and cholesterol transport on oxysterol-binding protein phosphorylation and golgi localization. *Journal of Biological Chemistry*, 273, 31621-31628
2. Stryer, L., Berg, J. M., & Tymoczko, J. L. (2007). *Biochemistry* (6th ed.). San Francisco: W.H. Freeman.
3. Carter, J. S. (2014). *Lipids: Fats, Oils, Waxes, etc.* Retrieved from University of Cincinnati Clermont College Biology:  
<http://biology.clc.uc.edu/courses/bio104/lipids.htm>
4. Featherstone, D. (2015). *Membrane Lipids*. Retrieved from University of Illinois at Chicago Department of Biological Sciences:  
<http://www.uic.edu/classes/bios/bios100/lectf03am/phospholipid.jpg>
5. Gobley, T. (1845). Recherches chimiques sur le jaune d'œuf. *Compte Rendu hebdomadaire Académie des Sciences*, 21, 766.
6. Aktas, M., Danne, L., Moller, P., & Narberhaus, F. (2014). Membrane lipids in *Agrobacterium tumefaciens*: biosynthetic pathways and importance for pathogenesis. *Frontiers in Plant Science*, 5. Retrieved from  
<http://journal.frontiersin.org/article/10.3389/fpls.2014.00109/full>
7. Avanti Polar Lipids, Inc. (2015). *1,2-dioleoyl-sn-glycero-3-phosphocholine*. Retrieved from Avanti Polar Lipids, Inc:  
[http://avantilipids.com/index.php?option=com\\_content&view=article&id=231&Itemid=207&catnumber=850375](http://avantilipids.com/index.php?option=com_content&view=article&id=231&Itemid=207&catnumber=850375)
8. Yorek, M. (1993). Biological Distribution. In G. Cevc, *Phospholipids Handbook* (pp. 745-775). Library of Congress.
9. Lange, Y. (1991). Disposition of intracellular cholesterol in human fibroblasts. *Journal of Lipid Research*, 32, 329-339.
10. Du, X., Brown, A., & Yang, H. (2015). Novel mechanisms of intracellular cholesterol transport: oxysterol-binding proteins and membrane contact sites. *Current Opinion in Cell Biology*, 35, 37-42.
11. Helle, S. C., Kanfer, G., Kolar, K., Lang, A., Michel, A. H., & Kornmann, B. (2013). Organization and function of membrane contact sites. *Biochimica et Biophysica Acta*, 1833, 2526-2541.

12. Levine, T. (2004). Short-range intracellular trafficking of small molecules across endoplasmic reticulum junctions. *TRENDS in Cell Biology*, *14*, 483-490.
13. Clapham, D. E. (2007). Calcium Signaling. *Cell*, *131*, 1047-1058.
14. Vance, J. E. (1990). Phospholipid synthesis in a membrane fraction associated with mitochondria. *Journal of Biological Chemistry*, *265*, 7248-7256.
15. Mesmin, B., Bigay, J., von Filseck, J. M., Lacas-Gervaise, S., Drin, G., & Antonny, B. (2013). A four-step cycle driven by PI(4)P hydrolysis directs sterol/PI(4)P exchange by the ER-Golgi tether OSBP. *Cell*, *155*, 830-843.
16. Olkkonen, V., & Levine, T. (2004). Oxysterol binding proteins: in more than one place at a time. *Biochemistry and Cellular Biology*, *82*, 87-98.
17. Olkkonen, V., & Lehto, M. (2004). Oxysterols and oxysterol binding proteins: role in lipid metabolism and atherosclerosis. *Annals of Medicine*, *36*, 562-572.
18. Koriyama, H., Nakagami, H., Katsuya, T., & Morishita, R. (2012). Functions of OSBP/ORP family proteins and their relation to dyslipidemia. In R. Kelishadi, *Dyslipidemia - From Prevention to Treatment* (pp. 129-140). InTech. Retrieved from <http://cdn.intechopen.com/pdfs-wm/27495.pdf>
19. Lehto, M., & Olkkonen, V. M. (2003). The OSBP-related proteins: a novel protein family involved in vesicle transport, cellular lipid metabolism, and cell signaling. *Biochimica et Biophysica Acta*, *1631*, 1-11.
20. Ridgway, N. D. (2010). Oxysterol-Binding Proteins. In J. R. Harris, *Cholesterol Binding and Cholesterol Transport Proteins* (Vol. 51, pp. 159-182). Springer Science + Business Media.
21. Im, Y. J., Raychaudhuri, S., Prinz, W. A., & Hurley, J. H. (2005). Structural mechanism for sterol sensing and transport by OSBP-related proteins. *Nature*, *437*, 154-158.
22. Raychaudhuri, S., Im, Y. J., Hurley, J. H., & Prinz, W. A. (2006). Nonvesicular sterol movement from plasma membrane to ER requires oxysterol-binding protein-related proteins and phosphoinositides. *Journal of Cell Biology*, *173*, 107-119.
23. de Saint-Jean, M., Delfosse, V., Douguet, D., Chicanne, G., Payrastra, B., Bourguet, W., Antonny, B., & Drin, G. (2011). Osh4p exchanges sterols for phosphatidylinositol 4-phosphate between lipid bilayers. *J. Cell. Biol.*, *195*, 965-978.

24. Schulz, T. A., Choi, M., Raychaudhuri, S., Mears, J. A., Ghirlando, R., Hinshaw, J., & Prinz, W. A. (2009). Lipid-regulated sterol transfer between closely apposed membranes by oxysterol-binding protein homologues. *Journal of Cell Biology*, *187*, 889-903.
25. Li, X., Rivas, M. P., Fang, M., Marchena, J., Mehrotra, B., Chaudhary, A., Feng, L., Prestwich, G. D., & Bankaitis, V. A. (2002). Analysis of oxysterol binding protein homologue Kes1p function in regulation of Sec14p-dependent protein transport from the yeast Golgi complex. *Journal of Cell Biology*, *157*, 63-77.
26. Fairn, G. D., Curwin, A. J., Stefan, C. J., & McMaster, C. R. (2007). The oxysterol binding protein Kes1p regulates Golgi apparatus phosphatidylinositol-4-phosphate function. *Proceedings of the National Academy of Sciences*, *104*, 15352-15357.
27. Goto, A., Liu, X., Robinson, C. A., & Ridgway, N. (2012). Multisite phosphorylation of oxysterol-binding protein regulates sterol binding and activation of sphingomyelin synthesis. *Molecular Biology of the Cell*, *23*, 3624-3635.
28. Hanada, K., Kumagai, K., Yasuda, S., Miura, Y., Kawano, M., Fukasawa, M., & Nishijima, M. (2003). Molecular machinery for non-vesicular trafficking of ceramide. *Nature*, *426*, 803-809.
29. D'Angelo, G., Polishchuk, E., Di Tullio, G., Santoro, M., Di Campli, A., Godi, A., West, G., Belawski, J., Chuang, C. C., van der Spoel, A. C., Platt, F. M., Hannun, Y. A., Polishchuk, R., Mattjus, P., & De Matteis, M. A. (2007). Glycosphingolipid synthesis requires FAPP2 transfer of glucosylceramide. *Nature*, *449*, 62-67.
30. Litvak, V., Dahan, N., Ramachandran, S., Sabanay, H., & Lev, S. (2005). Maintenance of the diacylglycerol level in the Golgi apparatus by the Nir2 protein is critical for Golgi secretory function. *Nature Cell Biology*, *7*, 225-234.
31. Lev, S. (2010). Non-vesicular lipid transport by lipid-transfer proteins and beyond. *Nature Reviews Molecular Cell Biology*, *11*, 739-750.
32. Kaiser, S. E., Brickner, J. H., Reilein, A. R., Fenn, T. D., Walter, P., & Brunger, A. T. (2005). Structural basis of FFAT motif-mediated ER targeting. *Structure*, *437*, 1035-1045.
33. Godi, A., Di Campli, A., Konstantakopoulos, A., Di Tullio, G., Alessi, D. R., Kular, G. S., Daniele, T., Marra, P., Lucocq, J. M., & De Matteis, M. A. (2004). FAPPs control Golgi-to-cell-surface membrane traffic by binding to ARF and PtdIns(4). *Nature Cell Biology*, *6*, 393-404.

34. Beh, C. T., McMaster, C. R., Kozminski, K. G., & Menon, A. K. (2012). A detour for yeast oxysterol binding proteins. *Journal of Biological Chemistry*, 287, 11481-11488.
35. Stefan, C. J., Manford, A. G., Baird, D., Yamada-Hanff, J., Mao, Y., & Emr, S. D. (2011). Osh proteins regulate phosphoinositide metabolism at ER-plasma membrane contact sites. *Cell*, 144, 389-401.
36. Hunter, T. (1995). Protein kinases and phosphatases: the yin and yang of protein phosphorylation and signaling. *Cell*, 80, 225-236.
37. Ciesla, J., Fraczyk, T., & Rode, W. (2011). Phosphorylation of basic amino acid residues in proteins: important but easily missed. *Acta Biochimica Polonica*, 58, 137-148.
38. Johnson, L. N. (2009). The regulation of protein phosphorylation. *Biochemical Society transactions*, 37, 627-641.
39. Goodman, S. (1999). *Carbohydrate Metabolism*. Retrieved from University of Kansas Medical Center: <http://www.kumc.edu/AMA-MSS/Study/carbohydrates.htm>
40. Storey, M. K., Byers, D. M., Cook, H. W., & Ridgway, N. D. (1998). Cholesterol regulates oxysterol binding protein (OSBP) phosphorylation and Golgi localization in Chinese hamster ovary cells: correlation with stimulation of sphingomyelin synthesis by 25-hydroxycholesterol. *The Biochemical Journal*, 15, 247-256.
41. Farfield Group Ltd. (2004). *Dual Polarisation Interferometry*. Retrieved from Farfield: [http://www.farfield-group.com/technology\\_dpi.asp](http://www.farfield-group.com/technology_dpi.asp)
42. Swann, M. J., Peel, L. L., Carrington, S., & Freeman, N. J. (2004). Dual-polarization interferometry: an analytical technique to measure changes in protein structure in real time, to determine the stoichiometry of binding events, and to differentiate between specific and nonspecific interactions. *Analytical Biochemistry*, 329, 190-198.
43. Morley, S., Cecchini, M., Zhang, W., Virgulti, A., Noy, N., Atkinson, J., & Manor, D. (2008). Mechanisms of ligand transfer by the hepatic tocopherol transfer protein. *Journal of Biological Chemistry*, 283, 17797-17804.
44. Zhang, W. X., Thakur, V., Lomize, A., Pogozeva, I., Panagabko, C., Cecchini, M., . . . Atkinson, J. (2011). The contribution of surface residues to membrane binding and ligand transfer by the  $\alpha$ -tocopherol transfer protein ( $\alpha$ -TTP). *Journal of Molecular Biology*, 405, 972-988.

45. Baptist, M., Panagabko, C., Nickels, J. D., Katsaras, J., & Atkinson, J. (2015). 2,2'-Bis(monoacylglycero) PO<sub>4</sub> (BMP), but Not 3,1'-BMP, increases membrane curvature stress to enhance  $\alpha$ -tocopherol transfer protein binding to membranes. *Lipids*, *50*, 323-328.
46. Dawson, P. A., Ridgway, N. D., Slaughter, C. A., Brown, M. S., & Goldstein, J. L. (1989). cDNA cloning and expression of oxysterol-binding protein, an oligomer with a potential leucine zipper. *Journal of Biological Chemistry*, *264*, 16798-16803.
47. Dawson, P. A., Van der Westhuyzen, D. R., Goldstein, J. L., & Brown, M. S. (1989). Purification of oxysterol binding protein from hamster liver cytosol. *Journal of Biological Chemistry*, *264*, 9046-9052.
48. Perry, R. J., & Ridgway, N. D. (2006). Oxysterol-binding protein and vesicle-associated membrane protein-associated protein are required for sterol-dependent activation of the ceramide transport protein. *Molecular Biology of the Cell*, *17*, 2604-2616.